



RESEARCH ARTICLE

10.1029/2018JB016369

Key Points:

- We reconstructed the Jurassic-Cretaceous plate tectonic history of the Caribbean Plate within the Mesozoic Panthalassa Ocean
- New paleomagnetic data indicate that northwestern Costa Rica was located within 10 degrees from the equator throughout the Cretaceous
- The western Caribbean subduction zone initiated in Late Cretaceous time, in an intraoceanic setting, breaking up lithosphere of at least 70 Myr old

Supporting Information:

- Supporting Information S1

Correspondence to:

L. M. Boschman,
lydian.boschman@usys.ethz.ch

Citation:

Boschman, L. M., van der Wiel, E., Flores, K. E., Langereis, C. G., & van Hinsbergen, D. J. J. (2019). The Caribbean and Farallon plates connected: Constraints from stratigraphy and paleomagnetism of the Nicoya Peninsula, Costa Rica. *Journal of Geophysical Research: Solid Earth*, 124, 6243–6266. <https://doi.org/10.1029/2018JB016369>

Received 11 JUL 2018

Accepted 28 MAY 2019

Accepted article online 4 JUN 2019

Published online 12 JUL 2019

©2019. The Authors.

This is an open access article under the terms of the Creative Commons Attribution-NonCommercial-NoDerivs License, which permits use and distribution in any medium, provided the original work is properly cited, the use is non-commercial and no modifications or adaptations are made.

The Caribbean and Farallon Plates Connected: Constraints From Stratigraphy and Paleomagnetism of the Nicoya Peninsula, Costa Rica

L. M. Boschman^{1,2} , E. van der Wiel¹, K. E. Flores^{3,4} , C. G. Langereis¹ , and D. J. J. van Hinsbergen¹

¹Department of Earth Sciences, Utrecht University, Utrecht, The Netherlands, ²Now at Department of Environmental Systems Science, ETH Zürich, Zürich, Switzerland, ³Department of Earth and Environmental Sciences, Brooklyn College of the City University of New York, Brooklyn, NY, USA, ⁴Department of Earth and Planetary Sciences, American Museum of Natural History, New York, NY, USA

Abstract Plate kinematic reconstructions play an essential role in our understanding of global geodynamics, but become increasingly difficult to constrain back in geological time due to the subduction of oceanic lithosphere. Here, we attempt to kinematically reconstruct the Cretaceous and older plate tectonic history of the Caribbean Plate within the Mesozoic Panthalassa (paleo-Pacific) Ocean. To this end, we present new paleomagnetic data from Jurassic and Cretaceous oceanic sedimentary and volcanic Large Igneous Province-related rocks of the Nicoya Peninsula and Murciélago Islands of northwestern Costa Rica. We use these data, in combination with constraints from marine magnetic anomalies to infer the age of the lithospheric basement, seismic tomography to locate deep-mantle plume generation zones, and general kinematic feasibility, to test different reconstruction scenarios connecting the Caribbean Plate to the Farallon Plate as restored from Pacific spreading records. Our resulting reconstruction implies that the western Caribbean subduction zone initiated around 100 Ma, in an intraoceanic setting, breaking up oceanic lithosphere of at least 70 Myr old.

1. Introduction

Plate kinematic reconstructions play an essential role in our understanding of global geodynamics, but become increasingly difficult to constrain back in geological time due to the subduction of oceanic lithosphere. The Panthalassa Ocean, which surrounded the supercontinent Pangea in Mesozoic times, is particularly difficult to restore (e.g., Boschman & van Hinsbergen, 2016). Marine magnetic anomalies in the present-day seafloor of the Pacific Ocean (Figure 1) document that the lithosphere of the Mesozoic and early Cenozoic (north)eastern Panthalassa Basin formed from spreading between the Pacific Plate and the conceptual Farallon Plate (Engelbreton et al., 1985; Wright et al., 2016). Except for the Juan de Fuca, Rivera, Cocos, and Nazca plates, which are presumed present-day remnants of the Farallon Plate, the absence of anomalies conjugate to the Jurassic-early Cenozoic anomalies of the Pacific Plate indicates that the vast majority of the Farallon Plate has been lost to subduction. Reconstruction of the kinematic history of the Farallon Plate therefore relies on indirect evidence such as the spreading history of the Pacific Plate (Engelbreton et al., 1985; Wright et al., 2016), geological and paleomagnetic records of the highly deformed continental margins of North and South America (Boschman, Garza, et al., 2018; Boschman, van Hinsbergen, et al., 2018; Johnston, 2001; Nokleberg, 2000; Tarduno et al., 1986; Tarduno & Alvarez, 1985), and interpretation of seismic tomography models that image subducted Farallon lithosphere (Boschman, van Hinsbergen, et al., 2018; Grand et al., 1997; Liu et al., 2008; Liu & Stegman, 2011; Sigloch & Mihalynuk, 2013; van der Meer et al., 2010, 2012, 2018).

When restoring the Mesozoic history of the Farallon plate, the Caribbean Plate is of particular interest. This plate, currently separated from the Cocos Plate by a subduction zone, is a remnant of Panthalassa lithosphere that instead of subducting - which happened to the north and south below the Americas - was captured between the Americas in Cretaceous time (Pindell et al., 1988). The bulk of the Caribbean Plate consists of oceanic lithosphere of unknown age covered by a thick layer of ~90-Ma oceanic plateau basalts of the Caribbean Large Igneous Province (CLIP; Burke, 1988; Burke et al., 1978; Donnelly et al., 1973;

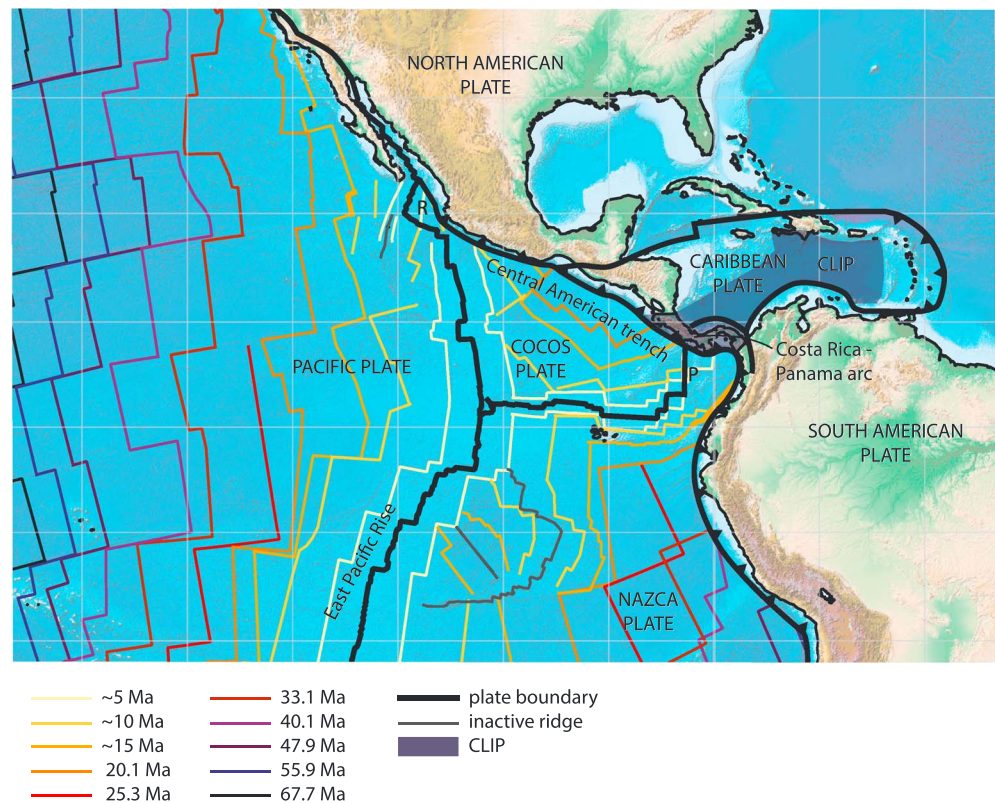


Figure 1. Tectonic map including the Caribbean, North and South American plates, the Pacific Plate, and its conjugates; the Rivera (R), Cocos, and Nazca plates. P: Panama fracture zone. Isochrons in the Pacific domain from Wright et al. (2016). Note the absence of old (>55 Ma) oceanic lithosphere east of the East Pacific Rise.

Saunders et al., 1996; Sinton et al., 1998, 2000; Figure 1). During break-up of Pangea, North and South America separated, resulting in the opening of the Proto-Caribbean Seaway that connected eastward to the Central Atlantic Ocean. Subsequent convergence between the Americas and the oceanic plates of the Panthalassa Ocean was associated with westward dipping subduction of this Proto-Caribbean lithosphere beneath the lithosphere of the future Caribbean Plate, which became progressively emplaced eastward from within the Panthalassa Ocean to its present position between the Americas (Burke et al., 1978; Pindell, 1985). The Caribbean lithosphere became a separate plate upon initiation of the western Caribbean subduction zone, associated with the Costa Rica-Panama arc. The age of this subduction initiation is debated and estimates vary from ~100 Ma (Whattam & Stern, 2015) to ~75 Ma (Buchs et al., 2010). The inferred close proximity in age of subduction initiation and extrusion of the CLIP has led several authors to suggest a causal relationship between the two phenomena, postulating that a mantle plume that generated the CLIP also induced western Caribbean subduction (Stern & Gerya, 2017; Whattam & Stern, 2015).

Kinematic reconstructions of the Caribbean Plate (e.g., Boschman et al., 2014; Burke, 1988; Burke et al., 1978; Pindell, 1985; Pindell et al., 1988; Pindell & Kennan, 2009) are based on geological records of collisions of the leading eastern edges of the Caribbean Plate with the North and South American continents since ~100 Ma and interactions between these plates along transform and subduction-dominated plate boundaries since then. Reconstructing the western margins, which were surrounded by now-subducted Panthalassa lithosphere, is more difficult, and for times prior to 100 Ma, when the Caribbean lithosphere was part of the independent Panthalassa plate system without a direct connection to the Indo-Atlantic plate system, its location and motion remains highly uncertain.

In this paper, we attempt to kinematically reconstruct the Cretaceous and older plate tectonic history of the Caribbean Plate within the Mesozoic Panthalassa Ocean. To this end, we present new paleomagnetic data from the oldest exposed rocks of the western Caribbean Plate: Jurassic and Cretaceous oceanic sedimentary and volcanic rocks of the Nicoya Peninsula and Murciélago Islands of northwestern Costa Rica. We use these

to test kinematic scenarios connecting the Caribbean Plate to the Farallon Plate as restored from Pacific spreading records, as a function of estimated ages of subduction initiation in the western Caribbean subduction zone. This establishes Mesozoic eastern Panthalassa plate motions in relation to the plate tectonic history of the continental plates making up the supercontinent Pangea.

2. Geological Setting

2.1. Tectonic Setting of the Nicoya Peninsula and Murciélago Islands

The western margin of the Caribbean Plate consists of the Central American land bridge and the Central American trench where eastward subduction consumes the Cocos and, south of the Panama fracture zone, the Nazca Plate (Figure 1). The modern Central American land bridge in the upper plate of this subduction zone hosts an active volcanic arc and consists from north to south of (1) the continental Chortís block of southern Guatemala and northern Honduras, which is bounded in the north by the left-lateral Motagua fault zone that forms the North American-Caribbean plate boundary (Donnelly et al., 1990; Rogers et al., 2007); (2) the Siuna terrane or Mesquito Composite Oceanic Terrane (MCOT) containing an oceanic basement, serpentinite matrix mélanges, and Mesozoic-Cenozoic arc volcanic rocks (Baumgartner et al., 2008; Venable, 1994); and (3) the oceanic Costa Rica-Panama block, consisting of mainly CLIP and arc-related magmatic rocks (Buchs et al., 2010; Gazel et al., 2009) and connecting to the northwestern Andes, which contains the diffuse plate boundary between the Caribbean and South American plates (Figures 1 and 2). Terrane nomenclature and boundaries within the northern part of the Central American land bridge (and offshore Nicaraguan Rise), as well as the interpreted tectonic histories of these terranes, are debated: the Siuna terrane (southern Nicaragua and northwesternmost Costa Rica, Figure 2, e.g., Boschman et al., 2014; Rogers et al., 2007; Sanchez et al., 2016; Venable, 1994) is considered to be a fragment of the Great Arc of the Caribbean (Burke, 1988)—an arc built on oceanic basement representing the leading edge of the Caribbean Plate—that collided with the continental Chortís block in Late Cretaceous time and has been part of the North American Plate since then. Baumgartner et al. (2008) on the other hand, named a larger area (also including southern Honduras, El Salvador, the southern half of the offshore Nicaraguan Rise, and the oceanic fore-arc in the west) the MCOT, which is defined as an assemblage of Mesozoic Franciscan-type mafic and ultramafic terranes of paleo-Pacific and arc origin. Based on a 139.2 ± 0.4 Ma phengite cooling age of a metamorphic block from the Siuna serpentinite mélange, this composite terrane is interpreted to have collided with continental Chortís in early Cretaceous time (Baumgartner et al., 2008; Flores et al., 2015).

The focus area of this study, the Nicoya Peninsula and Murciélago Islands, is located in the fore-arc region of the Central American subduction system, just south of the boundary between the MCOT/Siuna terrane and the Costa Rica-Panama block, the latter representing the arc associated with the western Caribbean subduction zone (Baumgartner et al., 2008; Figure 2). It is part of a fore-arc sliver that migrates trench parallel (northwestward) relative to the main Central American land bridge (Funk et al., 2009; Montero et al., 2017; Phipps Morgan et al., 2008). Just north of the Murciélago Islands, the Santa Elena Peninsula of northernmost Costa Rica exposes an ultramafic peridotite nappe thrust over an oceanic accretionary complex (Figure 2), interpreted as the remnants of a Cretaceous paleotrench (Baumgartner & Denyer, 2006; Escuder-Viruete & Baumgartner, 2014; Gazel et al., 2006), which likely represents the Costa Rica-Panama block-MCOT/Siuna terrane plate boundary.

In the early stages of subduction, the subduction zone along the western margin of the Caribbean Plate did not connect to the long-lived trenches along continental North (including Chortís) or South America as it does today. Instead, it was located within the Panthalassa realm and migrated eastward relative to the Americas. In the Boschman et al. (2014) reconstruction of the Caribbean region, which serves as a basis for this study, initiation of the western Caribbean subduction zone was modeled at 85 Ma, following the 88–80 Ma estimate of Pindell and Kennan (2009). This estimate is based on the oldest, Coniacian tuffaceous, arc-derived sedimentary rocks overlying the oceanic basement of the Nicoya and Santa Elena peninsulas of Costa Rica. However, other authors consider these sedimentary overlap assemblages to be unrelated to subduction in the western Caribbean subduction zone and correlate them to either another intraoceanic subduction zone (Baumgartner et al., 2008; Buchs et al., 2010) or subduction below the active southern margin of the North American Plate (Andjić et al., 2018). This age may thus not be representative for western Caribbean subduction initiation. Buchs et al. (2010) instead argued for 75–73 Ma protoarc formation, based

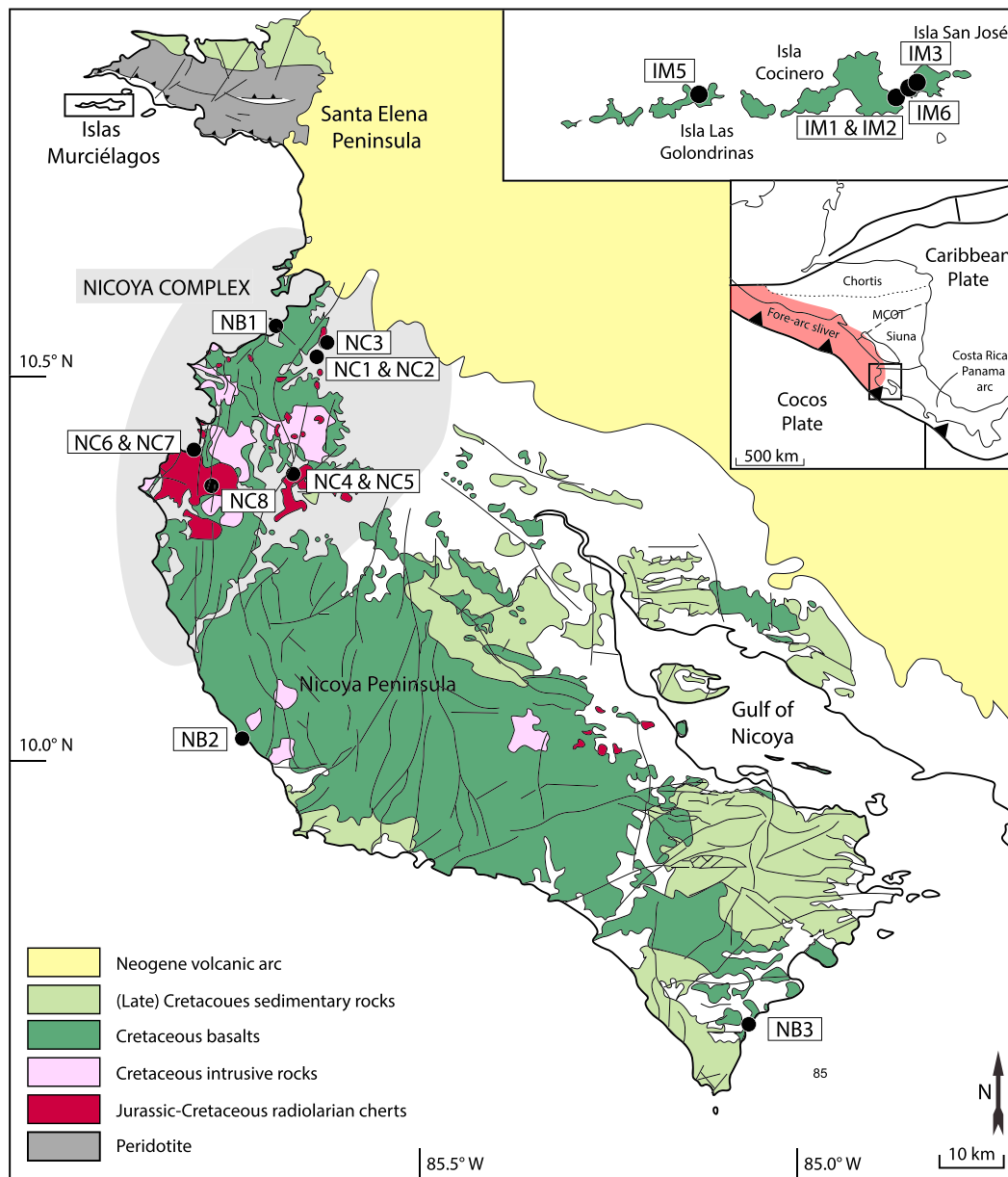


Figure 2. Geological map of the Nicoya Peninsula and the Murciélago Islands including sampling locations, modified from Whattam et al. (2016) and Andjić et al. (2018). Inset: Central American land bridge, including basement terranes.

on geochemical signatures (intermediate between plateau and arc) of the oldest arc magmatic rocks in Costa Rica and Panama. Independent from implications by their specific geochemical signature, the presence of 75–73 Ma arc volcanic rocks in Panama and Costa Rica indicates that subduction must have been underway at least by 75 Ma, making this the minimum age limit of subduction initiation. Subduction initiation may also be older; Whattam and Stern (2015) proposed a plume-induced subduction initiation model in which ~100 Ma subduction initiation was triggered by the same plume that extruded the CLIP.

2.2. Stratigraphy of the Nicoya Peninsula and Murciélago Islands

The Nicoya Peninsula exposes (1) folded ribbon-bedded radiolarian cherts of Bajocian-Bathonian, Oxfordian-Tithonian, Valanginian-Albian, and Coniacian-Santonian ages (Baumgartner et al., 2008; Denyer & Baumgartner, 2006), following the Baumgartner et al. (1995) zonation; (2) basaltic rocks, dated by $^{40}\text{Ar}/^{39}\text{Ar}$ geochronology at 139.1–132.9, 119.4–118.2, 110.6, and 94.7–89.7 Ma (Hauff et al., 2000;

Hoernle et al., 2004; Madrigal et al., 2016; Sinton et al., 1997); and (3) 89.3–77.2 Ma diabbases, gabbros, and plagiogranites ($^{40}\text{Ar}/^{39}\text{Ar}$ and U-Pb ages; Hauff et al., 2000; Madrigal et al., 2016; Sinton et al., 1997; Whattam et al., 2016; Figure 2). At contacts with intrusive rocks, radiolarian cherts show chilled margins and hydrothermal leaching indicating clear cross-cutting relationships (Baumgartner et al., 2008). The bulk of the magmatic rocks falls within the narrow range (~90 Ma) of radiometric ages from basaltic rocks of the CLIP elsewhere in the Caribbean region (Alvarado et al., 1997; Hauff et al., 1997, 2000; Hoernle et al., 2004; Kerr et al., 1997; Révillon et al., 2000; Sinton et al., 1997, 1998, 2000), and all Cretaceous magmatic rocks from the Nicoya Peninsula, including the pre-90 Ma ones, yield similar geochemical signatures, reflecting mixing between Mid-Ocean Ridge Basalt (MORB) and intraplate magmatism, which is interpreted as evidence for a shared plume-influenced mantle source (Hauff et al., 1997, 2000; Hoernle et al., 2004; Madrigal et al., 2016; Sinton et al., 1997).

Originally, all oceanic assemblages in northwest Costa Rica (including the Nicoya Peninsula) were termed “Nicoya Complex” (Dengo, 1962; Kuijpers, 1980). However, in more recent studies, the use of this term is restricted to the tectonic unit cropping out in the northwestern Nicoya Peninsula only (Figure 2; Andjić et al., 2018; Bandini et al., 2008; Denyer & Baumgartner, 2006; Denyer & Gazel, 2009). The Nicoya Complex is covered by middle Campanian-Maastrichtian shallow water carbonate deposits (ages based on planktonic foraminifera and rudists; Baumgartner-Mora & Denyer, 2002; Denyer et al., 2014; Pons et al., 2016). The central and southern part of the Nicoya Peninsula differs from the Nicoya Complex by the absence of Jurassic-Albian radiolarian cherts and ~139–133 Ma magmatic rocks. It is overlain by siliceous and bituminous black shales of the Loma Chumico Formation and Coniacian-Campanian pelagic to turbiditic sequences of the Sábana Grande and Nambí formations (ages based on radiolaria and $^{87}\text{Sr}/^{86}\text{Sr}$ dating on *Inoceramus* bivalve fossils; Bandini et al., 2008; Flores et al., 2003b; Flores, 2006; Schmidt-Effing, 1979). The Loma Chumico Formation is dated as Albian by ammonite occurrences (Astorga, 1997; Azéma et al., 1979). However, Coniacian-upper Campanian radiolaria have also been reported (Andjić et al., 2018). In the Gulf of Nicoya region, the magmatic basement is overlain by middle Turonian-Santonian pelagic and bituminous shales and arc-related tuffaceous debris flows of the Berrugate Formation (Bandini et al., 2008; Flores et al., 2003a, 2003b).

The archipelago of the Murciélago Islands is located north of the Nicoya Peninsula, just south of the Santa Elena Peninsula (Figure 2). These islands consist of tilted tholeiitic massive and pillow basalts, which yielded $^{40}\text{Ar}-^{39}\text{Ar}$ ages of 109.0 ± 2 Ma and 113.4 ± 3.5 Ma (Hauff et al., 2000; Madrigal et al., 2016). Geochemically, the Murciélago Islands basalts are almost identical to the CLIP and the older basaltic suites of the Nicoya Peninsula (Escuder-Viruet et al., 2015; Madrigal et al., 2015).

2.3. Previous Tectonic Interpretations

Interpretations of the formation of the Nicoya Complex can be broadly summarized in two categories. The first invokes that the Nicoya Complex formed as an accretionary complex, in which Large Igneous Province (LIP) and chert rocks of different ages were not deposited near each other, but were amalgamated from >1,000 km of now-subducted lithosphere (e.g., Galli-Olivier, 1979; Madrigal et al., 2016). A second category of models suggests that the Nicoya complex forms a deformed but overall coherent stratigraphy deposited on Panthalassa (Farallon) lithosphere. In the latter category, deformation of the cherts is thought to reflect disruption and detachment from their original basement during pulses of plume-related magmatism (Denyer & Baumgartner, 2006).

Independent of any model, the presence of Bajocian-Bathonian radiolarian cherts testifies to a Bajocian or pre-Bajocian oceanic basement on which the oldest rock assemblages now incorporated in the Nicoya Complex formed (Denyer & Baumgartner, 2006; Denyer & Gazel, 2009; Sinton et al., 1997). The absence of coarse detrital sediments and arc-derived rocks in the Jurassic-Early Cretaceous sequence implies that this lithospheric basement was not in close proximity to a continental margin or a subduction zone throughout its early history (Andjić et al., 2018). Accretionary complexes are generally characterized by more or less coherent, trenchward younging nappes consisting of both foreland (trench fill) sedimentation and far-traveled ocean plate stratigraphy separated by thrust faults (e.g., Matsuda & Isozaki, 1991). In the Nicoya complex, no such nappes, major thrust faults or younger trench fill deposits are observed (Denyer & Baumgartner, 2006) or suggested by the modern geomorphology. This forms a challenge for models that infer that the Nicoya Complex consists of accreted or amalgamated fragments of ocean plate stratigraphy and plateau remnants that were originally far apart.

The Murciélago Islands basalts are by some authors associated with the Santa Elena Nappe, exposed on the Santa Elena Peninsula to the north (Denyer & Gazel, 2009; Gazel et al., 2006). However, as no contact or clear lithological relation to the Santa Elena Nappe is present and the Murciélago Islands basalts contain a geochemical signature almost identical to CLIP magmas, other authors relate the Murciélago Islands basalts to the Nicoya Complex (Escuder-Viruet et al., 2015; Madrigal et al., 2015). Exclusive evidence on the tectonic relationship between the Murciélago Islands basalts, the Santa Elena Nappe, and the Nicoya Complex remains absent.

3. Sampling and Ages

We collected a total of 243 cores and 74 hand samples for paleomagnetic analysis, categorized in three groups: Murciélago Islands basalts (Islas Murciélagos, IM), Nicoya basalts (NB), and Nicoya cherts (NC). We obtained samples from three different islands of the Murciélago Bay: Isla Cocinero (IM1, IM2), Isla San José (IM3, IM6), and Isla Las Golondrinas (IM5). Except for IM2, where we took seven samples from a single lava, all samples are from individual pillow basalts (9, 17, 12, and 7 samples, respectively). Bedding orientations (strike 279, dip 75°N) are consistent throughout the islands and $^{40}\text{Ar}/^{39}\text{Ar}$ dating of intrapillow glass and whole rock matrix has yielded ages of 113.4 ± 3.5 Ma (Isla Las Golondrinas, Madrigal et al., 2016) and 109.0 ± 2.0 Ma (Isla Cocinero, Hauff et al., 2000), respectively.

We sampled the Nicoya basalts at sections of pillow basalts along the western coast of the peninsula, whereby each sample is from an individual pillow. To optimize the amount of geological time within each sample set in order to average paleosecular variation, we collected the samples at sections of hundreds of meters thick with the spacing between samples generally 5–10 m. At locality NB1, which is located between Playa del Coco and Punta Cacique, we obtained 76 cores from a ~500-m-long section. $^{40}\text{Ar}/^{39}\text{Ar}$ dating of these basalts yielded ages of 139.1 ± 1.1 (Hoernle et al., 2004) and 137.1 ± 2.5 Ma (Madrigal et al., 2016). At locality NB2, on the beach of Puerto San Juanillo, we obtained 67 samples from ~700 m of exposure. The pillow basalts are interbedded with thin layers of radiolarian chert, indicative of a significant amount of geological time within this section. $^{40}\text{Ar}/^{39}\text{Ar}$ dating yielded an age of 119.4 ± 1.1 Ma (Hoernle et al., 2004). At locality NB3, at the beach of Montezuma, we collected 46 samples from a ~500-m section of pillow basalts (NB3.1–3.13, 3.24–3.46) interbedded with fine grained sediments containing small grains of chert (NB3.14–3.23). Calcareous intrapillow sediments contain late Cenomanian-Turonian (~94 Ma) foraminifera (Tournon & Alvarado, 1997).

The sampled Mn-radiolarites occur as isolated and highly tectonized exposures on the northwestern Nicoya Peninsula. We sampled sites of 7–11 hand samples in stratigraphic order, generally within 1 or 2 m of exposure. All NC exposures belong to the Nicoya Complex and were previously dated by radiolarian biostratigraphy by Denyer and Baumgartner (2006). Sites NC1 and NC2 (eight and seven hand samples) were collected from a quarry located north of the town of Sardinal de Carrillo. This exposure is characterized by tight folds and generally steeply dipping strata (~70°). Radiolarian assemblages from this outcrop range from middle Oxfordian to early Tithonian (~155–145 Ma). Site NC3 (nine hand samples) is located 2 km farther north, near the town of Santa Rita. Radiolarites from this exposure contain late Barremian to early Aptian (~123–119 Ma) radiolarian assemblages. Sites NC4 and NC5 (10 and 9 hand samples) were collected from a heavily weathered and tectonized exposure located in Oratorio de Cartagena, containing the oldest radiolarian assemblage in the Nicoya Peninsula which is Bajocian in age (~174–166 Ma). Sites NC6 and NC7 (10 and 11 hand samples) were sampled in Punta Conchal. This locality is characterized by the occurrence of late Valanginian-Hauterivian to Aptian radiolarian assemblages (~133–111 Ma). At site NC6, we sampled both west and north dipping limbs of a fold. Finally, site NC8 (10 hand samples) was sampled from a small road-cut exposure near the village of Huacas, containing late Bajocian-early Bathonian (~167–164 Ma) radiolarian assemblages.

4. Methods

From basaltic rocks, we sampled typical paleomagnetic cores, 2.5 cm in diameter, with a gasoline-powered motor drill, and measured their orientation with an ASR OR-2 orientation device and Brunton compass. From cherts, we took oriented hand samples, and we drilled one to six cores per hand sample in the laboratory using a drill press. The cores were cut with a double blade circular saw into samples of 2.2-cm length.

Laboratory analyses were carried out at the Paleomagnetic Laboratory Fort Hoofddijk at Utrecht University in the Netherlands. Basalt samples were subjected to either stepwise thermal (TH) or alternating field (AF) demagnetization and chert samples to TH demagnetization only. Natural remanent magnetizations (NRMs) were measured on a 2G Enterprises SQUID cryogenic magnetometer. We used the following demagnetization steps: 0, 4, 8, 12, 16, 20, 25, 30, 35, 40, 45, 50, 60, 70, 80 mT for AF treatment, and 20, 100, 150, 200, 250, 300, 330, 360, 390, 420, 450, 480, 510, 540, 560, 580, 600, 620, 640, 660, 680 °C (or until complete demagnetization) for TH treatment. AF treatment samples were preheated at 150 °C to reduce effects of weathering on the NRM (van Velzen & Zijdeveld, 1995), and demagnetization was performed on an in-house developed robotized demagnetization device (Mullender et al., 2016). Sample interpretation and statistical analysis were performed in the online portal paleomagnetism.org (Koymans et al., 2016), using orthogonal vector diagrams (Zijderveld, 1967) and principal component analysis (Kirschvink, 1980). Because of the extraordinarily low sedimentation rate of radiolarian cherts (e.g., Matsuda & Isozaki, 1991), we calculated site mean directions from individual samples (instead of from hand samples means), to preserve all information on paleosecular variation (PSV) in the magnetization of the chert sites. Site means were calculated from virtual geomagnetic poles after a 45° cutoff (Johnson et al., 2008) using Fisher (1953) statistics. We calculated the N -dependent values of $A95_{\min}$ and $A95_{\max}$, following statistical procedures described in Deenen et al. (2011, 2014). Fold tests (Tauxe & Watson, 1994) and bootstrapped coordinate tests (Tauxe, 2010) were performed when applicable. All paleomagnetic results are summarized in Table 1, and data files can be found in the supporting information.

5. Paleomagnetic Results

5.1. Basalts

Demagnetization diagrams of NB1, NB2, and NB3 generally show two types of behavior. The majority (65/77 for NB1, 63/69 for NB2, and 43/44 for NB3) of the samples reveal an overprint at steps up to 20 mT or 210 °C and linear decay toward the origin at 40–60 mT or 580 °C (e.g., NB1.18A, NB1.48A, NB1.59A, NB2.10B, NB2.27, NB2.28, NB3.28A, and NB3.41A, Figures 3b–3d, 3f and 3g, and 3j and 3k). The rest of the samples, generally the weaker ones, reveal the same overprint but subsequently scatter around the origin instead of decaying toward it (e.g., NB1.2, NB2.1A, and NB3.7B, Figures 3a, 3e, and 3i). The latter samples are not interpreted. Initial intensities range between 10 mA/m and 30 A/m. In all three sites, inclinations scatter around zero, so both upward and downward directed inclinations are present. All directions (within the 45° cutoff) have northwest to southwestward declinations, indicating that there are no reversals recorded within sites NB1, NB2, and NB3. There is not sufficient variation in bedding throughout the sections to perform meaningful fold tests. The average (tilt-corrected) characteristic remanent magnetization (ChRM) directions are NB1: Dec $\pm \Delta D_x = 286.1 \pm 5.0^\circ$, Inc $\pm \Delta I_x = 7.7 \pm 9.9^\circ$, $n = 54$, $K = 16$, $A95 = 5.0$; NB2: Dec $\pm \Delta D_x = 228.3 \pm 5.3^\circ$, Inc $\pm \Delta I_x = 17.2 \pm 9.8^\circ$, $n = 42$, $K = 18.7$, $A95 = 5.2$; NB3: Dec $\pm \Delta D_x = 254.2 \pm 6.5^\circ$, Inc $\pm \Delta I_x = 10.2 \pm 12.7^\circ$, $n = 26$, $K = 20.1$, $A95 = 6.5$ (Table 1).

Demagnetization diagrams from IM1, IM3, IM5, and IM6 reveal a low-temperature/coercivity overprint and linear decay toward the origin at demagnetization steps up to 80 mT or 580 °C. ChRMs are generally interpreted at 16–50 mT or 360–500 °C (Figures 4a and 4c–4f). Initial intensities range from 0.5 to 20 A/m. Similar to NB1, NB2, and NB3, inclinations scatter around zero, and all declinations (within the 45° cutoff) are westward, indicating that there are no reversals recorded within sites IM1356. The average tilt-corrected ChRM direction is Dec $\pm \Delta D_x = 291.1 \pm 4.9^\circ$, Inc $\pm \Delta I_x = 3.8 \pm 9.7^\circ$, $n = 44$, $K = 22.1$ and $A95 = 4.9$. For samples from IM2, most of the magnetic signal is lost within the first four demagnetization steps, and therefore, ChRMs can only be interpreted in low temperature/coercivity steps (330–420 °C or 12–20 mT, Figure 4b). The resulting directions are significantly different from IM1356, and the interpreted ChRM directions have a k value of 28.9, indicating higher amounts of scatter than expected for samples from a single lava, which should represent a spot reading of the magnetic field (generally $k \ll 50$, e.g., Biggin et al., 2008). For these reasons, we exclude IM2 from further analysis.

The sampled rocks from sites NB2, NB3, and IM1356 formed during the Cretaceous normal superchron, and therefore, when assuming that the interpreted magnetization was acquired during formation of the rocks, the polarity of these samples must be normal. As a result, a southern hemisphere origin for NB2, NB3, and IM1356 can be excluded, and the westward declinations represent counterclockwise rotations.

Table 1
Paleomagnetic Results

Localities	Latitude (°N)	Longitude (°W)	Age	N	N45(is)	N45(tc)	Tilt-corrected										Rejected due to		
							Insitu												
					D	ΔD_x	I	ΔI_x	D	ΔD_x	I	ΔI_x	k	α_{95}	K	λ	A95min < A95 < A95max		
NB1	10.56755	85.69314	137.6 ± 1.8 Ma	65	56	54	296.4	5.3	12.7	10.2	286.1	5.0	7.7	9.9	10.2	6.4	16	3.9	2.4 < 5 < 6.6
NB2	10.02701	85.73885	119.4 ± 1.1 Ma	63	41	42	236.2	4.9	21.0	8.7	228.3	5.3	17.2	9.8	13.2	6.3	18.7	8.8	2.7 < 5.2 < 7.8
NB3	9.65157	85.06761	Cenomanian/ Turonian	43	27	26	256.0	6.6	6.5	13.1	254.2	6.5	10.2	12.7	13.7	7.9	20.1	5.2	3.3 < 6.5 < 10.5
IM1	10.85505	85.91023	109 ± 2 Ma	9	9	9	282.7	4.5	13.1	8.7	292.6	3.7	-0.1	7.4	106.9	5.0	197.0		5 > 3.7 < 20.5
IM3	10.85712	85.90699	109 ± 2 Ma	17	17	15	261.8	9.5	16.0	17.8	290.4	9.8	17.5	18.1	13.1	11.0	16.5		4.1 < 9.7 < 14.9
IM5	10.85741	85.93941	109 ± 2 Ma	11	11	11	289.4	10.5	13.0	20.0	291.0	12.2	-10.2	23.8	13.5	12.9	15.0		4.6 < 12.2 < 18.1
IM6	10.85683	85.90814	109 ± 2 Ma	7	6	6	280.1	9.8	11.5	18.9	290.4	6.8	1.9	13.6	43.9	10.2	97.2		5.9 < 6.8 < 26.5
IM1356	10.85524	85.91005	109 ± 2 Ma	44	42	41	277.3	5.2	14.8	9.9	291.1	4.9	3.8	9.7	14.7	6	22.1	1.9	2.7 < 4.9 < 7.9
IM2 ^a			109 ± 2 Ma	9	9	9	330.0	14.0	18.6	14.0	318.9	10.6	-39.0	13.8	28.9	9.7	28.3		5 < 9.8 < 20.5
NC1 ^a	10.52667	85.63943	Middle Oxfordian- early Tithonian	9			119.4	16.9	57.4	12.4				2.3	10.9	16.1			k too low, inconsistent with IM1356
NC2 ^a	10.52667	85.63943	Middle Oxfordian- early Tithonian	17			110.3	18.4	51.5	16.8				8.9	12.7	6.3			Negative foldtest
NC3 ^a	10.54177	85.63112	Late Barremian- early Aptian	26			88.7	28.4	54.9	22.8				2.9	20.3	2.5			K too low
NC4 ^a	10.3721	85.67124	Bajocian	22			5.4	9.8	29.5	15.4				10.4	10.1	11.8			Negative foldtest, indistinguishable from GAD
NC5 ^a	10.3721	85.67124	Bajocian	9			309.2	-26.9						1.0		1.0			K too low
NC6 ^a	10.40379	85.80329	Hauterivian- Aptian	21			186.6	28.1	38.1	37.1				2.5	28.1	2.5			K too low
NC7	10.40379	85.80329	Hauterivian- Aptian	24	22	23	219.1	7.3	-11.1	14.0	221.3	6.5	-2.3	12.9	14.2	8.3	22.8	-1.1	3.4 < 6.5 < 11.4
NC8 ^a	10.35625	85.7799	Middle Jurassic- Early Cretaceous	29			240.0	3.2	14.5	6.0				43.5	4.1	73.5			Synfolding, K too high

Note. N = number of interpreted demagnetized specimens; N45(is)/N45(tc) = number of specimens that fall within the 45° cutoff in in situ coordinates/after tilt correction; D = declination; I = inclination.

^aStatistical parameters on directions in insitu coordinates.

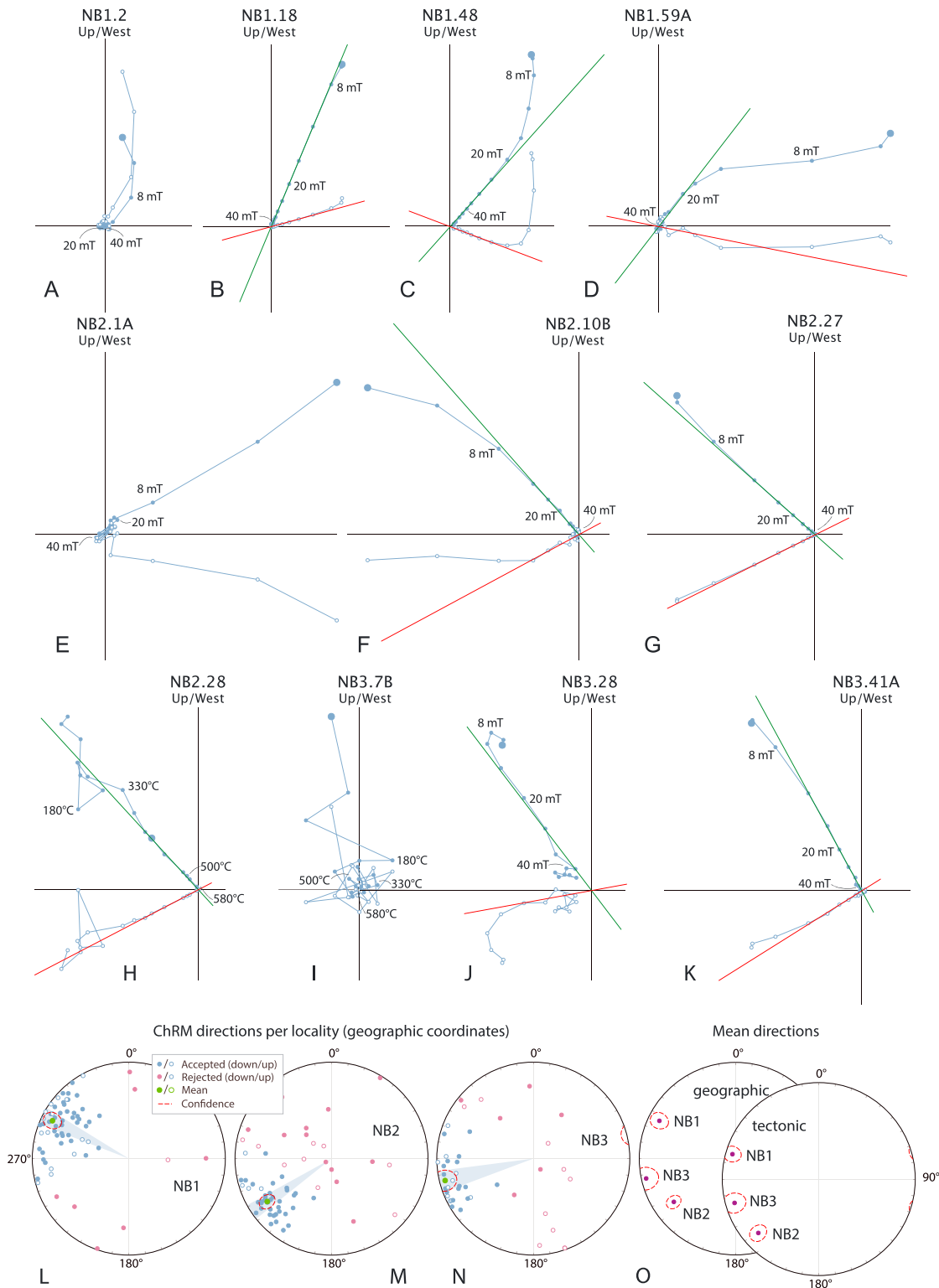


Figure 3. Paleomagnetic results from localities NB1, NB2, and NB3. (a–k) Orthogonal vector diagrams in geographic coordinates, closed (open) symbols for declination (inclination); (l–m) characteristic remanent magnetization (ChRM) directions per locality in geographic coordinates; and (n) mean directions in both geographic and tectonic coordinates.

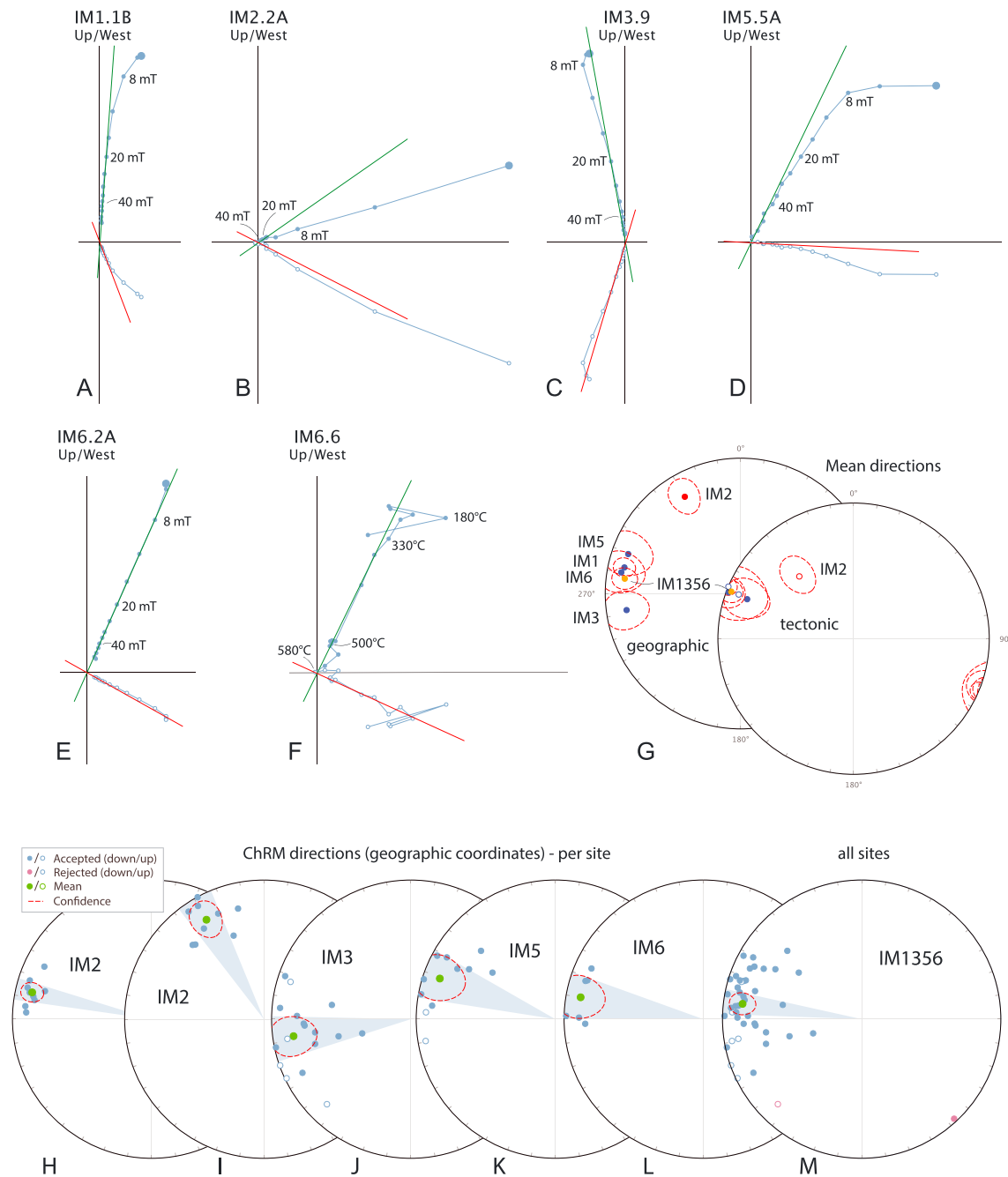


Figure 4. Paleomagnetic results from sites IM1-6. (a-f) Orthogonal vector diagrams in geographic coordinates, closed (open) symbols for declination (inclination); (g) mean directions per site in both geographic and tectonic coordinates; (h-l) characteristic remanent magnetization (ChRM) directions per site in geographic coordinates; and (m) ChRM directions for sites IM1356 in geographic coordinates.

Because demagnetization behavior and directions from NB1 are very similar to NB2 and NB3, we interpret these results to reflect counterclockwise rotations and a northern hemisphere origin as well.

5.2. Cherts

Contrary to the sampled pillow basalt sections, the sampled cherts lack any indication of stratigraphic younging direction. Therefore, correcting for bedding tilt yields two options: a smaller correction when the sediments are considered not to be overturned (hereafter: tc1) or a larger correction assuming overturned strata (tc2).

1. *NC1 and NC2*: Initial intensities range from 0.5 to 20 mA/m and ChRMs are interpreted between 500 and 680 °C (Figures 5a–5c). Directions from sites NC1 and NC2 share a common mean (Figure 6a). A series of fold tests (indeterminate for NC1, negative (tc1, best fit between –29% and 24% unfolding) or indeterminate (tc2) for NC2, and negative for NC1 and NC2 combined (best fit between –20% and 27% [tc1] or –41% and 14% [tc2] unfolding, Figure 6e) indicates that the magnetization is post-tilting and sites NC1 and NC2 are remagnetized.
2. *NC3*: Initial intensities range from 4 to 400 mA/m and ChRMs are generally interpreted in high temperature steps (550–680 °C, Figure 5d). Dispersion of the interpreted directions (Figure 6f) is essentially random ($K = 2.5$), which does not allow calculation of a meaningful mean direction. We reject this site from further analysis.
3. *NC4*: Initial intensities range from 0.6 to 10 mA/m and ChRMs are generally interpreted between 500 and 620 °C (Figures 5e and 5f). Variations in bedding orientations within the site allow for a fold test, which is negative (best fit between 7% and 20% [tc1] or –14% and –5% [tc2] unfolding, Figure 6h), and the mean direction in insitu coordinates is indistinguishable from the Geocentric Axial Dipole (GAD) field (inc: 20°, Figure 6g). We therefore interpret site NC4 to be recently remagnetized.
4. *NC5*: Due to the weathered nature of the rocks, many hand samples were lost during drilling in the laboratory, leaving only nine samples available for demagnetization. Initial intensities range from 35 to 85 mA/m and ChRMs were generally interpreted between 360 and 500 °C (Figures 5g and 5h). Interpreted directions yield a near-random distribution ($K = 1$, Figure 6i), and no meaningful site mean can be calculated. We exclude these results from further analysis.
5. *NC6*: Initial intensities range from 4 to 70 mA/m and ChRMs are generally interpreted between 330 and 580 °C (Figures 5i and 5j). Again, dispersion of the interpreted directions (Figure 6j) is too high ($K = 2.5$) to allow for calculation of a meaningful mean direction, and we reject this site from further analysis.
6. *NC7*: Initial intensities range from 4 to 70 mA/m. Demagnetization behavior varies: some samples contain three components (a low-temperature north-directed overprint, an intermediate component, and a high-temperature component trending toward the origin, e.g., NC7.6IIB, Figure 5k), other samples contain a single component (e.g., NC7.9IA, Figure 5l). The intermediate component (~200–400 °C) represents a postfolding magnetization (best fit between –49% and 58% [tc1], tc2 is indeterminate). ChRMs (the high-temperature or single component) are generally interpreted between 330 and 580 °C, yielding both normal and reversed directions (Figure 6k). The polarity changes follow a stratigraphic pattern: reversals are recorded between samples NC7.2 and NC7.3 and between NC7.6 and NC7.8. Both the reversal test and fold test are positive (best fit between 42% and 150% [tc1], tc2 is indeterminate, Figure 6l). The absence of control on hemispheric origin, polarity, or younging direction of the sampled sediments is not problematic for this site, as both tilt corrections (tc1 and tc2) yield directions with a common mean. Furthermore, both possible inclinations (2.3° or –2.3°) fall within each other's uncertainty limits ($\Delta I_x = 12.9$). Figure 7 and Table 1 include NC7 corrected with tc1 and in conjunction with results from NB and IM, representing counterclockwise rotations, resulting in a lower hemispheric origin (paleolatitude: –1.1°). The average tilt-corrected ChRM direction of NC7 is Dec $\pm \Delta D_x = 221.3 \pm 6.5^\circ$, Inc $\pm \Delta I_x = -2.3 \pm 12.9^\circ$, $n = 23$, $K = 22.8$, and the distribution of ChRMs satisfies the quality criteria of representing PSV (A95min = 3.4 < A95 = 6.5 < A95max = 11.4).
7. *NC8*: Demagnetizations from NC8 show consistent linear decay toward the origin at ~620–680 °C. ChRMs are interpreted between 360 and 680 °C and initial intensities range between 10 and 20 mA/m (Figures 5m and 5n). Fold tests are indeterminate (tc1) or indicate that acquisition of the magnetization was synfolding (best fit between 22% and 78% unfolding, tc2, Figure 6n), and the dispersion parameter is 73.5 (in insitu coordinates). Such a high K value on a site of sedimentary rocks indicates that a limited amount of secular variation is recorded, which is in line with a (rapid) remagnetization during folding.

5.3. Summary of Paleomagnetic Results

Due to the unavailability of fold and reversal tests for sites NB1, NB2, NB3, and IM1356, we cannot exclude that their ChRM directions represent a shared remagnetization, which would explain the absence of reversals in NB1. However, the absence of reversals in NB2, NB3, and IM1356 is consistent with the age of the rocks and magnetization acquisition during the Cretaceous normal superchron, and for all sites, the distributions of ChRMs satisfy the quality criteria of representing PSV (Table 1). We conclude that the magnetizations of NB1, NB2, NB3, and IM1356 are potentially primary. ChRM directions from NC7

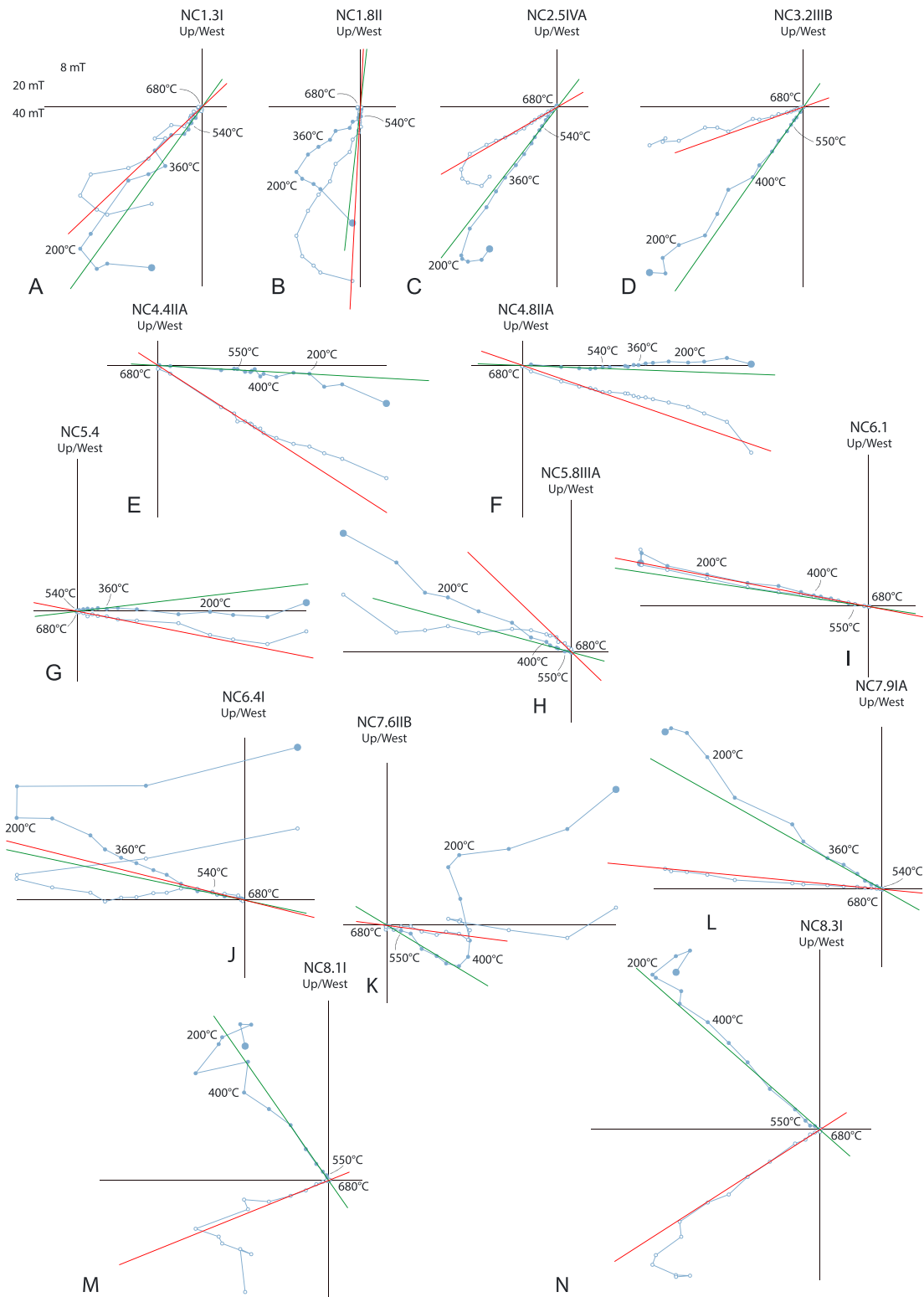


Figure 5. Orthogonal vector diagrams of sites NC1-8 in geographic coordinates, closed (open) symbols for declination (inclination).

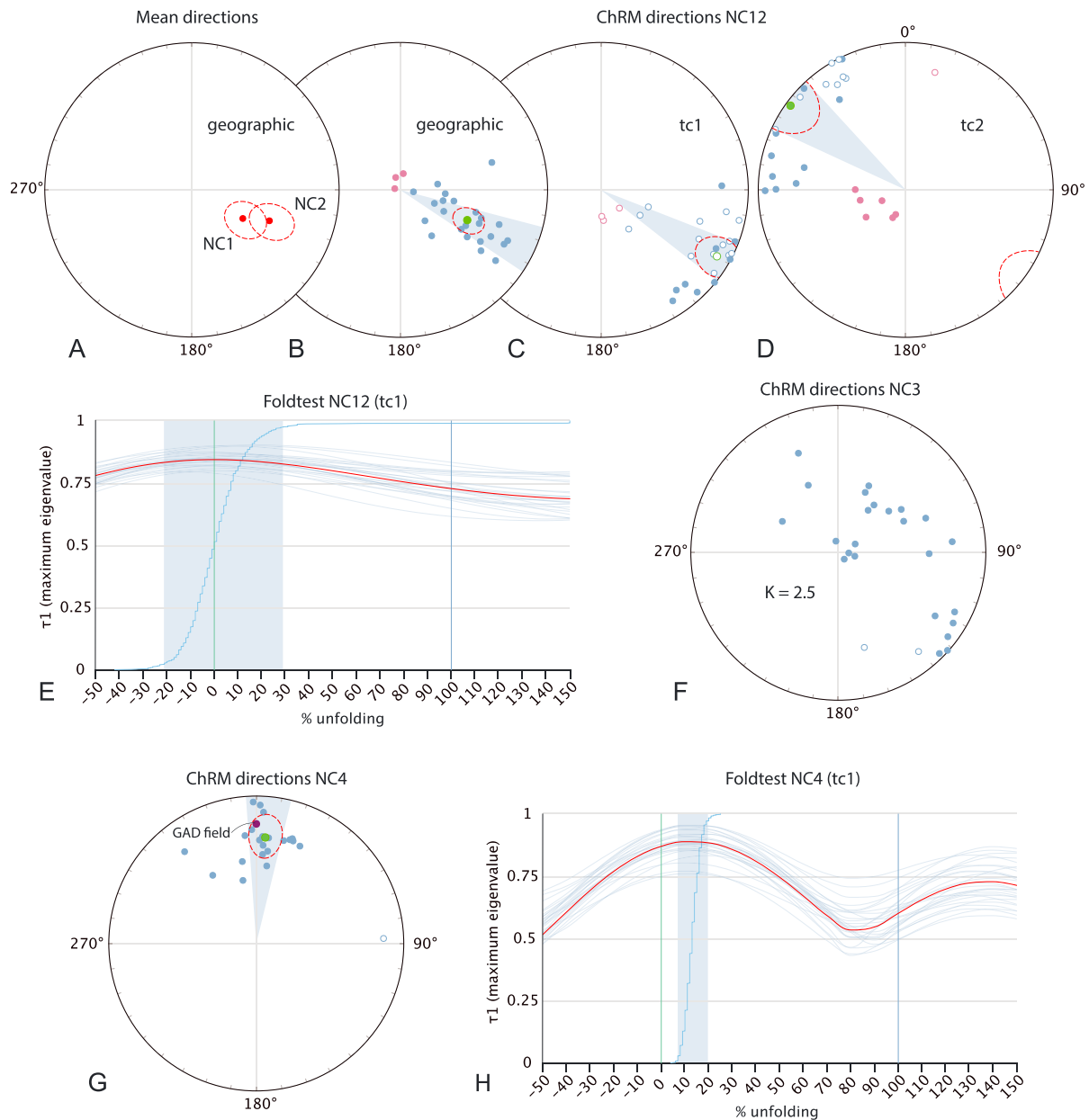


Figure 6. (a) Mean directions of sites NC1 and NC2, sharing a CTMD; (b–d) characteristic remanent magnetization (ChRM) directions of sites NC1 and NC2 in geographic and tectonic (tc1 and tc2) coordinates; (e) bootstrapped foldtest of sites NC1 and NC2: cumulative distribution function (with confidence interval in light blue) based on 1,000 bootstraps (average of bootstraps in red); (f) ChRM directions of site NC3; (g) ChRM directions of site NC4, including the GAD field in purple; (h) bootstrapped foldtest of site NC4: cumulative distribution function (with confidence interval in light blue) based on 1,000 bootstraps (average of bootstraps in red); (i–j) ChRM directions of sites NC5 and NC6; (k) ChRM directions of site NC7 containing both normal and reversed distributions; (l) bootstrapped foldtest of site NC7; (m) ChRM directions of site NC8; (n) bootstrapped foldtest of site NC8.

are highly likely to represent a primary magnetization: ChRMs satisfy the quality criteria of representing PSV, reversals are present and follow a stratigraphic pattern, and both the fold and reversal tests are positive. All other cherts sites yielded unsuccessful results. The results of NC7 are potentially affected by inclination shallowing due to compaction after acquisition of the magnetization. However, if present, such an effect of compaction is largest at midrange latitudes (40°–50°N or S), and very minor around the poles and equator. Correcting for inclination shallowing by using a typical compaction factor for fine-

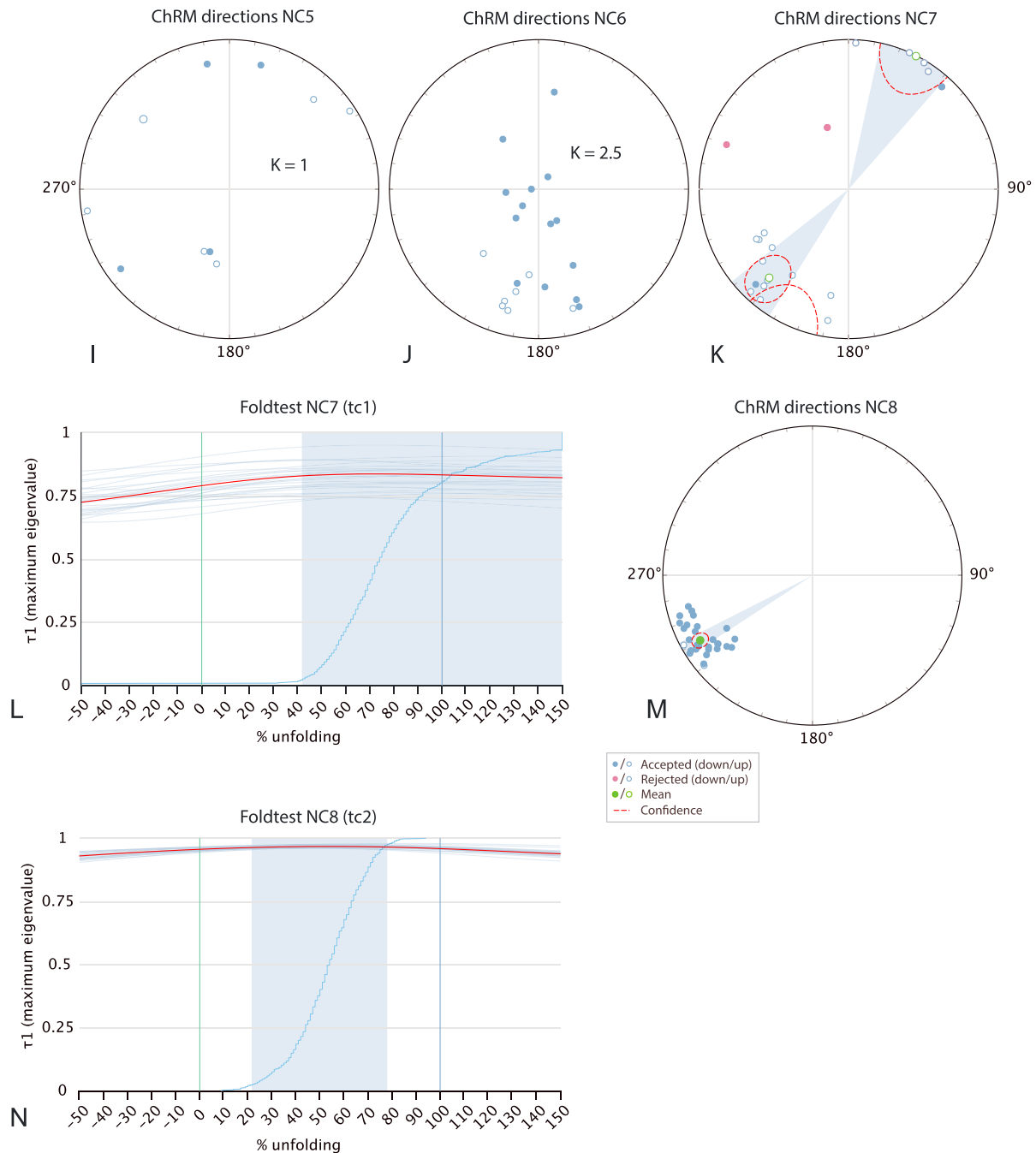


Figure 6. (continued)

grained sedimentary rocks (0.6–0.7) would steepen the inclination of NC7 only slightly, from $\pm 2.3^\circ$ to $\pm 3.3^\circ$ – 3.8° (Figure 7).

The paleomagnetic data from successful sites ([potentially] primary) indicate that the rock assemblages of the Nicoya Peninsula and Murciélago Islands formed within 10° of the equator during the Cretaceous. The consistent southwest to northwest directed declinations demonstrate a regional counterclockwise vertical axis rotation. However, significant variations in declination between sites indicate smaller, local rotations as well, probably due to local faulting (Figure 7). Previous paleomagnetic studies on younger (Campanian-Maastrichtian to Paleocene) rocks of the Nicoya Peninsula (Di Marco et al., 1995; Gose, 1983) yielded similar paleolatitudes (within 15° of the equator), but different rotations. Declinations of these younger rocks are

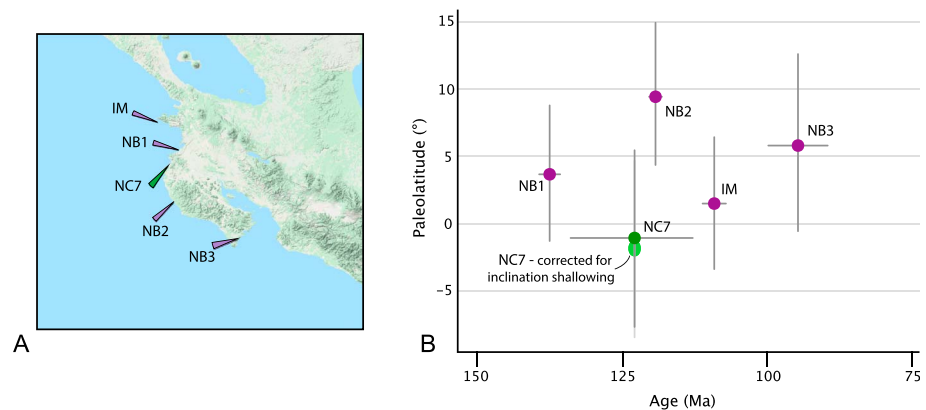


Figure 7. Paleomagnetic data from the Nicoya Peninsula and the Murciélago Islands. (a) Sampling locations and declinations with confidence parachutes (D_x); (b) paleolatitudes.

around zero, indicating that the counterclockwise rotation documented by the west directed declinations of this study occurred in Late Cretaceous times.

6. Discussion

6.1. Tectonic Interpretation of the Nicoya Peninsula

Our study attempts to kinematically link the Caribbean Plate with the oceanic plates of the Panthalassa Ocean in Mesozoic times. To this end, the Jurassic and Cretaceous rock record of the Nicoya Peninsula and Murciélago Islands is the most promising archive to constrain such a reconstruction, but this requires that this rock record is an integral part of the lithosphere of the western Caribbean Plate. This, however, is not beyond controversy and first requires discussion as to what extent rocks exposed on the Nicoya Peninsula and Murciélago Islands may be far-traveled, accreted exotic fragments, as recently suggested by Madrigal et al. (2016). Based on geochemistry, these authors interpreted the Cretaceous basalts exposed on the Nicoya Peninsula to represent small fragments of three separate LIPs (the ~140 Ma Nicoya I LIP and ~120 Ma Nicoya II LIP that formed at the Farallon-Pacific ridge, and the ~90 Ma CLIP). The Madrigal et al. (2016) plate tectonic model hinges on the assumption that it is unlikely or impossible for oceanic plateau material spanning ~50 Myr to have been extruded on the same location on a moving oceanic plate. Madrigal et al. (2016) therefore proposed that the different LIP fragments formed above the plume generation zone at the edge of the Large Low Shear-wave Velocity Province (LLSVP) below the Pacific Ocean as imaged in modern mantle structure, and were later accreted and amalgamated to form the Nicoya Complex. This scenario requires that the LIP fragments are currently separated by former subduction thrusts that consumed the hundreds of kilometers of oceanic basement that would have originally been present between the LIPs. Such a tectonic model would require the presence of typical ocean plate stratigraphy sequences, consisting of oceanic basement, pelagic sediments, and trench fill deposits, forming accretionary complexes separated by major thrust faults (Isozaki et al., 1990). However, no trench fill deposits or major thrust faults have been documented between the different basalt and chert exposures. The Nicoya Complex may thus rather be regarded as a coherent part of the upper, Caribbean Plate. Furthermore, in the Madrigal et al. (2016) model, no Bajocian or older lithosphere is present in the equatorial eastern Panthalassa Ocean to form the basement of the Nicoya Complex.

The alternative interpretation, in which the Nicoya Peninsula represents an integral part of the Farallon, and later, Caribbean Plate, implies the in situ buildup of ~50 Myr of plume-related magmatism. As shown by Torsvik et al. (2010), it is not uncommon for relatively small areas to contain a long history of plume-induced magmatism. Regions that have been located in proximity to the edge of an LLSVP for long periods of time (such as Southern Africa, southern Central Australia, or West Africa) contain plume-related magmatic rocks covering tens to even hundreds of millions of years and may contain large and also small-volume plume-related volcanic rocks. Hence, we argue that there is no direct necessity for the Nicoya basalts to represent separate LIP remnants that formed at large distances from each other, as long as Nicoya was located in close proximity to the edge of the LLSVP between ~140 and 90 Ma. We therefore chose the

kinematically simpler scenario and reconstruct the Nicoya Peninsula and the Murciélago Islands as a single coherent tectonic block. We follow the interpretation of Denyer and Baumgartner (2006) and interpret the Nicoya Peninsula rock assemblages to have formed on (pre-)Bajocian crust on which Bajocian and younger radiolarian cherts were deposited and multiple pulses of plume-related magmatism disrupted the original basement structures. The complex remained in this intraplate setting until initiation of the western Caribbean subduction zone immediately to its west and arrival at the southern margin of the MCOT/Siuna terrane in Late Cretaceous time, after which it was covered by tuffaceous arc-derived sediments and shallow water carbonates (Andjić et al., 2018; Denyer & Baumgartner, 2006). In the following kinematic analysis, we test under which conditions this interpretation aligns with the available geological and paleomagnetic data.

6.2. Kinematic Analysis

We develop a plate kinematic model that incorporates the Caribbean Plate into the Panthalassa plate system for the Mesozoic, prior to the initiation of the western Caribbean subduction zone. To this end, we explore connections of the Caribbean Plate to the plates reconstructed in the eastern Panthalassa Ocean at the time of subduction initiation in the western Caribbean subduction zone and test the reconstruction against paleomagnetic data. This analysis is challenging as a result of uncertainties in (1) the post-subduction initiation reconstruction of the Caribbean Plate relative to the North and South American plates; (2) reconstruction of the Farallon Plate relative to the Pacific Plate; (3) reconstruction of the position of the Panthalassa plate system relative to the Indo-Atlantic plate system, which relies prior to 83 Ma on independent mantle reference frames for both systems each with its own uncertainties; and (4) the age of initiation of the western Caribbean subduction zone.

As basis for our reconstruction, we use the GPlates (Boyden et al., 2011) reconstruction of the Caribbean region of Boschman et al. (2014; updated for Chortis based on Molina Garza et al., 2017) and add a polygon containing the Murciélago Islands and Nicoya Peninsula. First, we reconstruct a $\sim 90^\circ$ counterclockwise rotation of the Nicoya Peninsula and Murciélago Islands between 80 and 100 Ma, following our paleomagnetic results. The sedimentary assemblages overlying the Nicoya Peninsula are thought to record the Late Cretaceous collision with, or juxtaposition against, the southwestern margin of the North American Plate represented by the MCOT/Siuna terrane (Andjić et al., 2018; Baumgartner et al., 2008). In the reconstruction of Boschman et al. (2014), this area was considered to be the westernmost part of the Great Arc of the Caribbean and was therefore reconstructed as part of the leading edge of the Caribbean Plate colliding with continental Chortís at 85 Ma. If, on the other hand, this area is interpreted as the MCOT, it represents the southernmost part of the North American Plate and the southern tip of the western North American continental margin subduction zone since ~ 140 Ma. Although this debated area is currently juxtaposed to the Murciélagos Islands/Nicoya region, the different interpretations (and their implications) do not affect tectonic reconstruction of the Murciélagos Islands/Nicoya region. In both scenarios (illustrated in the final reconstruction), the Nicoya Peninsula, which represents the northwestern most part of the CLIP and (future) Caribbean Plate arrives at the southern margin of the MCOT/Siuna terrane at 88 Ma, thereby fulfilling stratigraphic constraints.

Next, we construct a Pacific-Farallon-Phoenix plate system using the isochrons of the Pacific Plate of Wright et al. (2016) and create a conjugate set of Farallon isochrons east of it, assuming symmetrical spreading, thereby constructing Pacific-Farallon plate motions. Similarly, we create Phoenix Plate isochrons conjugate to the southern (E-W oriented) Mesozoic isochrons of the Pacific Plate and construct Pacific-Phoenix plate motions. As relative Farallon-Pacific and Phoenix-Pacific plate motions are now established, so is the rate and direction of spreading between the Farallon and Phoenix plates. Even though the exact geometry (i.e., location of former ridge and transform segments) of the Farallon-Phoenix isochrons cannot be determined, we create hypothetical sets of isochrons for this spreading history, assuming symmetrical spreading and using minimal transform offsets.

In the next step in our analysis, we attach the Caribbean Plate to the reconstructed Farallon Plate for times prior to subduction initiation in the western Caribbean subduction zone, which marks the onset of relative Farallon-Caribbean motion and the birth of the Caribbean Plate. For times after 83 Ma, this is relatively straightforward, as the Pacific Plate was connected through Antarctica to the Indo-Atlantic plate circuit (e.g., Wright et al., 2016). For times prior to 83 Ma, this connection is absent and relative plate motions

SI Age (Ma)	Mantle reference	Age lithospheric basement (Ma)	Overlap North American - Caribbean Plate	Paleomagnetic data	Proximity LLSVP (140-110 Ma)
75	VdM		<input type="checkbox"/> overlap	<input checked="" type="checkbox"/> good fit	
	O'N	<input type="checkbox"/> 154-168	<input type="checkbox"/> overlap	<input checked="" type="checkbox"/> good fit	<input checked="" type="checkbox"/> <10° pre-95 Ma
	D		<input type="checkbox"/> overlap	<input checked="" type="checkbox"/> good fit	
85	VdM	<input type="checkbox"/> 154-168	<input type="checkbox"/> overlap	<input checked="" type="checkbox"/> permitted	<input checked="" type="checkbox"/> <10° pre-100 Ma
	O'N	<input checked="" type="checkbox"/> 180-185	<input type="checkbox"/> overlap	<input checked="" type="checkbox"/> permitted	<input checked="" type="checkbox"/> <10° pre-120 Ma
	D	<input checked="" type="checkbox"/> 180-185	<input type="checkbox"/> overlap	<input type="checkbox"/> no fit	<input checked="" type="checkbox"/> <10° pre-120 Ma
90	VdM	<input checked="" type="checkbox"/> ~168	<input checked="" type="checkbox"/> <200 km overlap	<input checked="" type="checkbox"/> permitted	<input checked="" type="checkbox"/> <10° pre-105 Ma
	O'N	<input checked="" type="checkbox"/> 185-190	<input type="checkbox"/> overlap	<input checked="" type="checkbox"/> permitted	<input checked="" type="checkbox"/> <10° pre-130 Ma
	D	<input checked="" type="checkbox"/> >190	<input type="checkbox"/> overlap	<input type="checkbox"/> no fit	<input checked="" type="checkbox"/> <10° pre-130 Ma
100	VdM	<input checked="" type="checkbox"/> 168-180	<input checked="" type="checkbox"/> no overlap	<input checked="" type="checkbox"/> permitted	<input checked="" type="checkbox"/> <10° pre-112 Ma
	O'N	<input checked="" type="checkbox"/> ~190	<input checked="" type="checkbox"/> no overlap	<input checked="" type="checkbox"/> permitted	<input type="checkbox"/> >10°
	D	<input checked="" type="checkbox"/> >190	<input checked="" type="checkbox"/> no overlap	<input type="checkbox"/> no fit	<input type="checkbox"/> >10°
110	VdM	<input checked="" type="checkbox"/> ~190	<input checked="" type="checkbox"/> no overlap	<input type="checkbox"/> no fit	<input checked="" type="checkbox"/> <10° pre-130 Ma
	O'N	<input checked="" type="checkbox"/> >190	<input checked="" type="checkbox"/> no overlap	<input type="checkbox"/> no fit	<input type="checkbox"/> >10°
	D	<input checked="" type="checkbox"/> >190	<input checked="" type="checkbox"/> <200 km overlap	<input type="checkbox"/> no fit	<input type="checkbox"/> >10°

Preferred reconstruction →

Figure 8. Results of testing the 15 different reconstructions against independent data sets. For the reconstructions with subduction initiation at 75 Ma, whereby the Caribbean Plate is connected to the Farallon Plate after 83 Ma, the results of the tests “Age lithospheric basement” and “Proximity LLSVP” do not vary between the different mantle frames, because at 75 Ma the full reconstruction is connected through the plate circuit. The position of the Nicoya Peninsula relative to Farallon isochrons and the edge of the large low shear-wave velocity province does therefore not vary.

can exclusively be estimated by placing both Panthalassa and Indo-Atlantic plate systems in mantle reference frames. For the pre-83 Ma Panthalassa plate system, we use absolute plate motions of the Pacific Plate (as published in Müller et al., 2016), based on the Pacific fixed hot spot frame of Wessel and Kroenke (2008; 0–144 Ma). Assuming hotspot fixity is a simplification: Wessel and Kroenke (2009) and Konrad et al. (2018) have demonstrated changes in interhot spot distances, which the fixed hot spot frame does not account for. Nevertheless, for pre-Late Cretaceous times, the Wessel and Kroenke (2008) frame provides the only available constraint on plate motions of the Pacific Plate. We use the finite rotation poles from Müller et al. (2016). These authors published a smoothed version of the Wessel and Kroenke (2008) frame for 83–140 Ma, in which cumulative 0–83 Ma Indo-Atlantic hotspot motion is accounted for by connecting the Pacific hotspots to Indo-Atlantic hotspots at 83 Ma. Finite rotations for 83–140 Ma were then calculated by using selected stage poles from Wessel and Kroenke (2008).

For the post-83 Ma Panthalassa system and the Indo-Atlantic plate system, we test three different frames; the moving hotspot frames of Doubrovine et al. (2012; 124–0 Ma) and O'Neill et al. (2005; 140–0 Ma) and the slab-fitted frame of van der Meer et al. (2010; 300–0 Ma). To test the implications of different subduction initiation estimates, we attach the Caribbean Plate to the Farallon Plate at five different ages: 110, 100, 90, 85, and 75 Ma, resulting in a total of 15 possible reconstructions, the differences depending on the choice of mantle frame and subduction initiation age.

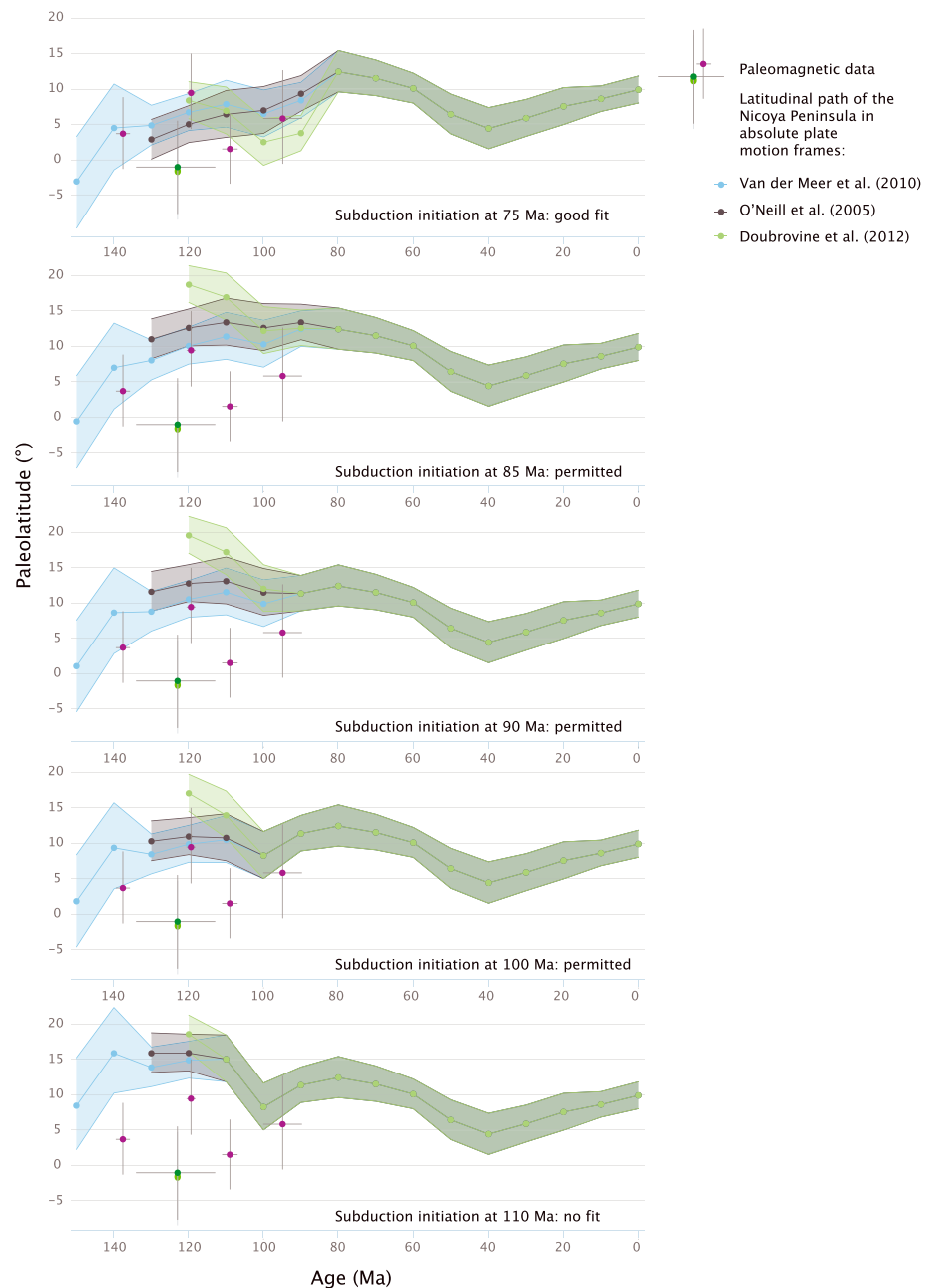


Figure 9. Paleomagnetic data compared to the expected paleolatitudes of the Nicoya Peninsula as predicted by the 15 different reconstructions, calculated for a reference location within the Nicoya Peninsula (10.1°N , 85.5°W). Reference values as predicted by the global apparent polar wander path of Torsvik et al. (2012).

We then test the 15 possible reconstructions against parameters not used to build the reconstructions above. These include (a) the kinematic feasibility of Caribbean lithosphere motion relative to the North American Plate (including the MCOT and the Chortis block) for times prior to subduction initiation. In reconstructions toward the younger end of the western Caribbean subduction initiation spectrum, an overlap between the northern margin of the Caribbean Plate and the southern margin of the North American Plate is present at $\sim 100\text{--}80$ Ma, whereas reconstructions with older subduction initiation ages yield no or little overlap (Figure 8); (b) the age of reconstructed Farallon lithosphere at the location of the Nicoya Peninsula, which should be at least Bajocian (~ 170 Ma) in age given the oldest radiolarian cherts on the Nicoya Peninsula. We consider reconstructions in which the Nicoya complex is located southwest of the 168 Ma isochron (on <168

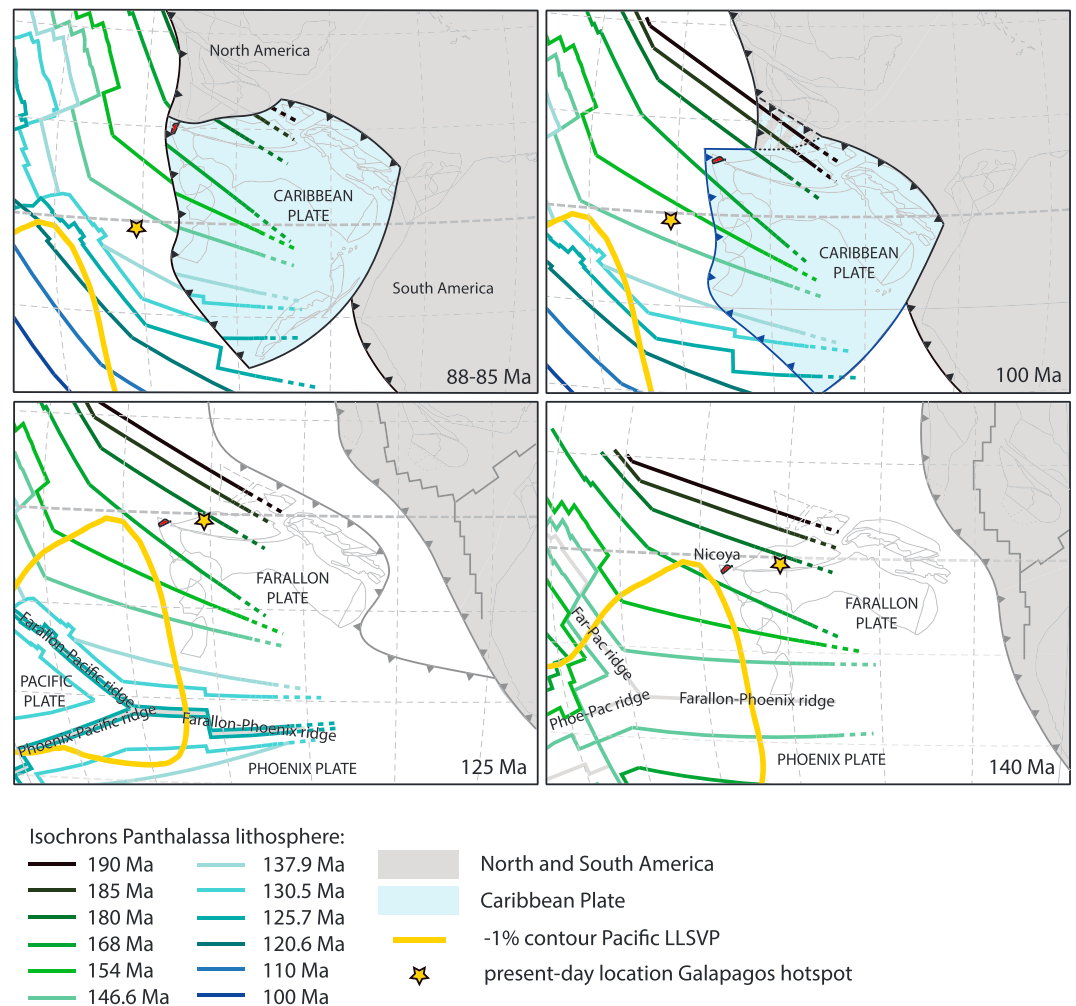


Figure 10. Reconstruction of the Caribbean region in the mantle stationary reference frame of van der Meer et al. (2010), with subduction initiation at 100 Ma. Outline large low shear-wave velocity province (LLSVP) is the -1% contour line (within this line: $>1\%$ slower than average mantle) of the SMEAN shear wave velocity model (Becker & Boschi, 2002) at 2,800-km depth (from Torsvik et al., 2006). Dashed: Siuna terrane (part of Caribbean Plate); dotted: MCOT (part of North American Plate); 140–125 Ma: the Nicoya Peninsula, located at the northwestern tip of the future Caribbean Plate, is close to the edge of the Pacific LLSVP; 100 Ma: subduction initiation in the western Caribbean subduction zone; 88 Ma: Nicoya is located adjacent to the southwestern margin of the North American Plate (MCOT). Euler poles for the Caribbean Plate and the Nicoya/Murciélagos block can be found in the supporting information.

Ma crust) less plausible. A good match exists between the age of the reconstructed Farallon basement underlying the reconstructed Nicoya Peninsula and the oldest radiolarian cherts now included in the Nicoya complex for all reconstructions, except for those with a 75 Ma subduction initiation age (Figure 8); (c) paleomagnetic data from the Nicoya Peninsula and Murciélagos Islands (Figures 7 and 9); and (d) proximity of the Nicoya Peninsula to the edge of the Pacific LLSVP at the time of extrusion of plateau basalts.

For the paleomagnetic test, we use the tool on paleomagnetism.org developed by Li et al. (2017) that allows testing whether Euler-pole based tectonic reconstructions agree with paleomagnetic data. To this end, we compute Euler poles in 10-Myr steps for the Nicoya Peninsula relative to Africa for all 15 reconstructions and calculate the global apparent polar wander path of Torsvik et al. (2012) into coordinates of the Nicoya Peninsula. In doing so, we switch from a reconstruction of plate motions relative to the lower mantle (that depends on the choice of mantle frame for the pre-83 Panthalassa plate system and the Indo-Atlantic plate system) to a reconstruction of plate motions relative to the spin axis, which enables comparison to paleomagnetic data. The paleolatitudes, declinations, and inclinations are computed for a reference point within the

Nicoya Peninsula (10.1°N, 85.5°W). The paleomagnetic data yield a better fit for reconstructions with younger subduction initiation ages (Figures 8 and 9).

Finally, we test whether the Nicoya Peninsula is in close proximity (within 10°, as are most reconstructed LIPs, Torsvik et al., 2006) to the edges of the Pacific LLSVP during the phases of LIP basalt extrusion (~139–133, ~120–110, and ~95–83 Ma). In all 15 reconstructions, the ~100–90 Ma position of the Nicoya Peninsula (i.e., during CLIP emplacement) is (>1,000 km) east of the edge of the Pacific LLSVP, as is the present-day position of the Galápagos hotspot (~850 km). For the two older pulses of LIP magmatism at ~139–133 and ~120–110 Ma, the Nicoya peninsula restores closer to the LLSVP edges with younger western Caribbean subduction initiation ages (Figure 8).

Summarizing all four tests, kinematic feasibility and the required age of the lithospheric basement point toward old (>100 Ma) subduction initiation ages, whereas the paleomagnetic data and LLSVP-proximity are better in line with young subduction initiation ages (<90/85 Ma). The first two of these tests are the most conclusive: overlap between two continental terranes or the absence of (pre-)Bajocian crust yields simply impossible reconstructions. The latter two are less robust, due to uncertainties in the nature of the magnetic signal (primary or remagnetized—except for NC7), and the uncertain allowance of 10° distance from the LLSVP. The reconstruction in the mantle reference frame of van der Meer et al. (2010) with a subduction initiation age of 100 Ma provides the optimal result, in full agreement with the first two tests, and permitted by the latter two (Figures 8 and 10).

6.3. Implications for Western Caribbean Subduction Initiation

Our attempt to reconstruct the Mesozoic history of the Caribbean Plate within the Panthalassa Ocean yields a reconstruction that is kinematically feasible, provides a sound explanation for the buildup of 50 Myr of LIP material on the Nicoya Peninsula, and is in line with the available paleomagnetic data. This successful reconstruction indicates that the lithosphere underlying the Caribbean Plate formed due to Farallon-Phoenix spreading prior to initiation of the western Caribbean subduction zone and predicts that the Caribbean Plate is underlain by Jurassic lithosphere that increases in age toward the northeast.

These findings have important implications for the setting of formation of the western Caribbean subduction zone. Current dynamic and kinematic models widely infer that intraoceanic subduction initiation occurs along preexisting weakness zones at or close to active plate boundaries (transform faults and mid-ocean ridges; Agard et al., 2007; Duretz et al., 2016; Hall et al., 2003; Leng & Gurnis, 2011; Maffione et al., 2015; Maffione & van Hinsbergen, 2018; Stern, 2004; Stern & Gerya, 2017; Stern et al., 2012). In our reconstruction, the western Caribbean subduction zone formed at high angles to inferred Farallon-Phoenix isochrons and, given reconstruction uncertainties, may have formed parallel to fracture zones. However, with a subduction initiation age of ~100 Ma, the western Caribbean subduction zone formed in lithosphere that was at least 70 Myr old at that time and was located far away from active intraoceanic plate boundaries. Such old lithosphere is strong, cold, and therefore a surprising locus for intraoceanic subduction initiation.

In this respect, our reconstruction may provide additional support for the proposal of Whattam and Stern (2015) for plume-induced subduction initiation (Gerya et al., 2015) in the western Caribbean region. The eruption of the CLIP basalts around the Caribbean region is mostly ~90–85 Ma in age (see compilation in Whattam & Stern, 2015), somewhat younger than the best fit subduction initiation age of 100 Ma estimated here. This may be the result of reconstruction uncertainty, but on the other hand, numerical models have shown that the dynamic effects of plume rise on plates may precede LIP emplacement by ~10–15 Myr (van Hinsbergen et al., 2011). We therefore concur that the Caribbean region may be an elegant test case for plume-induced subduction initiation within an old oceanic lithosphere.

7. Conclusions

We developed a plate kinematic model that incorporates the Caribbean Plate into the Panthalassa plate system for Mesozoic times by connecting the Caribbean lithosphere to the Farallon Plate prior to subduction initiation in the western Caribbean subduction zone. This reconstruction is nonunique due to the uncertain age of subduction initiation in the western Caribbean subduction zone, as well as differences between available mantle reference (absolute plate motion) frames. We therefore developed 15 reconstruction scenarios, which we then tested against four parameters not used to build the reconstructions: (1) kinematic feasibility;

(2) age of the Farallon plate lithosphere at the location of the restored Nicoya Peninsula, which must have been older than the oldest (Bajocian) radiolarian cherts of the peninsula; (3) newly presented paleomagnetic data; and (4) proximity to the edge of the Pacific LLSVP during the 50 Myr period of buildup of LIP material in the Nicoya Complex. Many paleomagnetic sites from the Nicoya Peninsula and Murciélago Islands of northwestern Costa Rica did not yield meaningful results, but the few sites with a (potentially) primary magnetic signal indicate that these terranes formed within 10° of the equator in Cretaceous time and consistently underwent counterclockwise vertical axis rotations. Considering all four tests, the reconstruction in the mantle reference frame of van der Meer et al. (2010) with a subduction initiation age of 100 Ma provides the optimal result. This implies that the western Caribbean subduction zone initiated in an intraoceanic setting around the time of emplacement of the Caribbean Large Igneous Province, breaking up oceanic lithosphere of at least 70 Myr old.

Acknowledgments

This project was supported by NWO grant 824.01.004 to L. M. Boschman, a NWO Vidi grant 864.11.004 to D. J. J. van Hinsbergen, and Brooklyn College start-up funds to K. E. Flores. Logistics for the fieldwork were supported by the Universidad de Costa Rica with project 830-B0-242 and ED-2700 to Percy Denyer. We thank M. M. Chavarria and R. Blanco of the Área de Conservación Guanacaste for their valuable support during field work in the Santa Rosa National Park, M. Salazar Alvarado and I. Boschini López of the Dirección de Geología y Minas for their support exporting the samples, and A. Bando of Brooklyn College for her help in the field and laboratory. All paleomagnetic data (supporting information Data Set S1) can be viewed in the online portal paleomagnetism.org.

References

- Agard, P., Jolivet, L., Vrielynck, B., Burov, E., & Monie, P. (2007). Plate acceleration: the obduction trigger? *Earth and Planetary Science Letters*, 258(3-4), 428–441. <https://doi.org/10.1016/j.epsl.2007.04.002>
- Alvarado, G. E., Denyer, P., & Sinton, C. W. (1997). The 89 Ma Tortugal komatiitic suite, Costa Rica: Implications for a common geological origin of the Caribbean and Eastern Pacific region from a mantle plume. *Geology*, 25(5), 439–442. [https://doi.org/10.1130/0091-7613\(1997\)025<0439:TMTKSC>2.3.CO;2](https://doi.org/10.1130/0091-7613(1997)025<0439:TMTKSC>2.3.CO;2)
- Andjić, G., Baumgartner, P. O., & Baumgartner-Mora, C. (2018). Rapid vertical motions and formation of volcanic arc gaps: Plateau collision recorded in the forearc geological evolution (Costa Rica margin). *Basin Research*, 30(5), 863–894. <https://doi.org/10.1111/bre.12284>
- Astorga, A. (1997). El puente-istmo de América Central y la evolución de la Placa Caribe (con énfasis en el Mesozoico). *Profil*, 12, 1–201.
- Azéma, J., Tournon, J., & Sornay, J. (1979). Presencia de amonites del Albiano Superior en las formaciones del Complejo de Nicoya. El yacimiento de Loma Chumico, provincia de Guanacaste, Costa Rica. *Informe Semestral del Instituto Geográfico Nacional*, 2, 71–76.
- Bandini, A. N., Flores, K., Baumgartner, P. O., Jackett, S. J., & Denyer, P. (2008). Late Cretaceous and Paleogene Radiolaria from the Nicoya Peninsula, Costa Rica: A tectonostratigraphic application. *Stratigraphy*, 5(1), 3–21. <Go to ISI>://WOS:000256639800002
- Baumgartner, P. O., & Denyer, P. (2006). Evidence for middle Cretaceous accretion at Santa Elena Peninsula (Santa Rosa Accretionary Complex), Costa Rica. *Geologica Acta*, 4(1-2), 179–191. <Go to ISI>://WOS:000237710200010
- Baumgartner, P. O., Flores, K., Bandini, A. N., Girault, F., & Cruz, D. (2008). Upper Triassic to Cretaceous radiolaria from Nicaragua and Northern Costa Rica—The Mesquito composite oceanic terrane. *Ofoliti*, 33(1), 1–19. <Go to ISI>://WOS:000257392900001
- Baumgartner, P. O., O'Dogherty, L., Goričan, Š., Urquhart, E., Pilleveit, A., & De Wever, P. (1995). Middle Jurassic to Lower Cretaceous radiolaria of Tethys: Occurrences, systematics, biochronology. International Association of Radiolarian Paleontologists, INTERRAD Jurassic-Cretaceous Working Group, 37–685.
- Baumgartner-Mora, C., & Denyer, P. (2002). Campanian-Maastrichtian limestone with larger foraminifera from Peña Bruja Rock (Santa Elena Peninsula). *Revista Geológica de América Central*, 26, 85–89.
- Becker, T. W., & Boschi, L. (2002). A comparison of tomographic and geodynamic mantle models. *Geochemistry, Geophysics, Geosystems*, 3(1), 1003. <https://doi.org/10.1029/2001GC000168>
- Biggin, A. J., van Hinsbergen, D. J. J., Langereis, C. G., Straathof, G. B., & Deenen, M. H. L. (2008). Geomagnetic secular variation in the Cretaceous Normal Superchron and in the Jurassic. *Physics of the Earth and Planetary Interiors*, 169(1-4), 3–19. <https://doi.org/10.1016/j.pepi.2008.07.004>
- Boschman, L. M., Garza, R. S. M., Langereis, C. G., & van Hinsbergen, D. J. (2018). Paleomagnetic constraints on the kinematic relationship between the Guerrero terrane (Mexico) and North America since Early Cretaceous time. *Geological Society of America Bulletin*, 130(7-8), 1131–1142. <https://doi.org/10.1130/B31916.1>
- Boschman, L. M., van Hinsbergen, D. J., Kimbrough, D. L., Langereis, C. G., & Spakman, W. (2018). The dynamic history of 220 million years of subduction below Mexico: A correlation between slab geometry and overriding plate deformation based on geology, paleomagnetism and seismic tomography. *Geochemistry, Geophysics, Geosystems*, 19, 4649–4672. <https://doi.org/10.1029/2018GC007739>
- Boschman, L. M., & van Hinsbergen, D. J. J. (2016). On the enigmatic birth of the Pacific Plate within the Panthalassa Ocean. *Science Advances*, 2(7). <Go to ISI>://WOS:000381805300014
- Boschman, L. M., van Hinsbergen, D. J. J., Torsvik, T. H., Spakman, W., & Pindell, J. L. (2014). Kinematic reconstruction of the Caribbean region since the Early Jurassic. *Earth-Science Reviews*, 138, 102–136. <https://doi.org/10.1016/j.earscirev.2014.08.007>
- Boyd, J., Müller, R. D., Gurnis, M., Torsvik, T., Clark, J. A., Turner, M., et al. (2011). Next-generation plate-tectonic reconstructions using GPlates. In *Geoinformatics: Cyberinfrastructure for the Solid Earth Sciences* (pp. 95–114). Cambridge: Cambridge University Press. <https://doi.org/10.1017/CBO9780511976308.008>
- Buchs, D. M., Arculus, R. J., Baumgartner, P. O., Baumgartner-Mora, C., & Ulianov, A. (2010). Late Cretaceous arc development on the SW margin of the Caribbean Plate: Insights from the Golfito, Costa Rica, and Azuero, Panama, complexes. *Geochemistry, Geophysics, Geosystems*, 11, Q07S24. <https://doi.org/10.1029/2009GC002901>
- Burke, K. (1988). Tectonic evolution of the Caribbean. *Annual Review of Earth and Planetary Sciences*, 16(1), 201–230. <https://doi.org/10.1146/annurev.ea.16.050188.001221>
- Burke, K., Fox, P. J., & Şengör, A. M. C. (1978). Buoyant ocean floor and the evolution of the Caribbean. *Journal of Geophysical Research*, 83(B8), 3949. <https://doi.org/10.1029/JB083iB08p03949>
- Deenen, M. H. L., Langereis, C. G., van Hinsbergen, D. J., & Biggin, A. J. (2014). Erratum: Geomagnetic secular variation and the statistics of palaeomagnetic directions. *Geophysical Journal International*, 197(1), 643–643. <https://doi.org/10.1093/gji/ggu021>
- Deenen, M. H. L., Langereis, C. G., van Hinsbergen, D. J. J., & Biggin, A. J. (2011). Geomagnetic secular variation and the statistics of palaeomagnetic directions. *Geophysical Journal International*, 186(2), 509–520. <https://doi.org/10.1111/j.1365-246X.2011.05050.x>
- Dengo, G. (1962). *Estudio geológico de la región de Guanacaste*. Costa Rica: Instituto Geográfico de Costa Rica.

- Denyer, P., Aguilar, T., & Montero, W. (2014). Cartografía geológica de la península de Nicoya, Costa Rica: Estratigrafía y tectónica: Editorial UCR.
- Denyer, P., & Baumgartner, P. O. (2006). Emplacement of Jurassic-Lower Cretaceous radiolarites of the Nicoya Complex (Costa Rica). *Geologica Acta*, 4(1-2), 203–218. <Go to ISI>://WOS:000237710200012
- Denyer, P., & Gazel, E. (2009). The Costa Rican Jurassic to Miocene oceanic complexes: Origin, tectonics and relations. *Journal of South American Earth Sciences*, 28(4), 429–442. <https://doi.org/10.1016/j.jsames.2009.04.010>
- Di Marco, G., Baumgartner, P. O., & Channell, J. E. (1995). *Late Cretaceous—Early Tertiary paleomagnetic data and a revised tectonostratigraphic subdivision of Costa Rica and western Panama, Geological Society of America Special Paper* (Vol. 295).
- Donnelly, T. W., Horne, G. S., Finch, R. C., & López-Ramos, E. (1990). Northern Central America; the Maya and chortis blocks. *The Geology of North America*, 11, 37–76.
- Donnelly, T. W., Melson, W., Kay, R., & Rogers, J. W. (1973). Basalts and dolerites of Late Cretaceous age from the Central Caribbean. In *Initial reports of the Deep Sea Drilling Project* (Chap. 30, pp. 989–1011). Washington, DC: US Government Printing Office.
- Dobrovine, P. V., Steinberger, B., & Torsvik, T. H. (2012). Absolute plate motions in a reference frame defined by moving hot spots in the Pacific, Atlantic, and Indian oceans. *Journal of Geophysical Research*, 117, B09101. <https://doi.org/10.1029/2011JB009072>
- Duret, T., Agard, P., Yamato, P., Ducassou, C., Burov, E. B., & Gerya, T. V. (2016). Thermo-mechanical modeling of the obduction process based on the Oman ophiolite case. *Gondwana Research*, 32, 1–10. <https://doi.org/10.1016/j.gr.2015.02.002>
- Engelbreton, D. C., Cox, A., & Gordon, R. G. (1985). *Relative motions between oceanic and continental plates in the Pacific basin, Geological Society of America Special Papers* (Vol. 206). <https://doi.org/10.1130/SPE206-p1>
- Escuder-Viruete, J., & Baumgartner, P. O. (2014). Structural evolution and deformation kinematics of a subduction-related serpentinite-matrix mélange, Santa Elena peninsula, northwest Costa Rica. *Journal of Structural Geology*, 66, 356–381. <https://doi.org/10.1016/j.jsg.2014.06.003>
- Escuder-Viruete, J., Baumgartner, P. O., & Castillo-Carrión, M. (2015). Compositional diversity in peridotites as result of a multi-process history: The Pacific-derived Santa Elena ophiolite, northwest Costa Rica. *Lithos*, 231, 16–34. <https://doi.org/10.1016/j.lithos.2015.05.019>
- Fisher, R. (1953). Dispersion on a sphere. *Proceedings of the Royal Society A: Mathematical, Physical and Engineering Sciences*, 217(1130), 295–305. <https://doi.org/10.1098/rspa.1953.0064>
- Flores, K., Denyer, P., & Aguilar, T. (2003a). Nueva propuesta estratigráfica: Geología de la hoja Abangares Guanacaste, Costa Rica. *Revista Geológica de América Central*, 29, 127–136.
- Flores, K., Denyer, P., & Aguilar, T. (2003b). Nueva propuesta estratigráfica: Geología de las hojas Matambú y Talolinga, Guanacaste, Costa Rica. *Revista Geológica de América Central*, 28, 131–138.
- Flores, K. E. (2006). Jurassic-Late Cretaceous oceanic crustal terranes and arc-derived sediments south Chortis Block (NE Nicaragua to NW Costa Rica)—Preliminary results of two key areas: Nicoya Peninsula and Siuna District. (DEA Thesis), Université de Lausanne, (107 p.)
- Flores, K. E., Skora, S., Martin, C., Harlow, G. E., Rodríguez, D., & Baumgartner, P. O. (2015). Metamorphic history of riebeckite-and aegirine-augite-bearing high-pressure-low-temperature blocks within the Siuna Serpentine Mélange, northeastern Nicaragua. *International Geology Review*, 57(5-8), 943–977. <https://doi.org/10.1080/00206814.2015.1027747>
- Funk, J., Mann, P., McIntosh, K., & Stephens, J. (2009). Cenozoic tectonics of the Nicaraguan depression, Nicaragua, and Median Trough, El Salvador, based on seismic-reflection profiling and remote-sensing data. *Geological Society of America Bulletin*, 121(11-12), 1491–1521. <https://doi.org/10.1130/B26428.1>
- Galli-Olivier, C. (1979). Ophiolite and island-arc volcanism in Costa-Rica. *Geological Society of America Bulletin*, 90(5), 444–452. <Go to ISI>://WOS:A1979GS86000003
- Gazel, E., Carr, M. J., Hoernle, K., Feigenson, M. D., Szymanski, D., Hauff, F., & van den Bogaard, P. (2009). Galapagos-OIB signature in southern Central America: Mantle refertilization by arc-hot spot interaction. *Geochemistry, Geophysics, Geosystems*, 10, Q02S11. <https://doi.org/10.1029/2008GC002246>
- Gazel, E., Denyer, P., & Baumgartner, P. O. (2006). Magmatic and geotectonic significance of Santa Elena Peninsula, Costa Rica. *Geologica Acta*, 4(1-2), 193–202. <Go to ISI>://WOS:000237710200011
- Gerya, T. V., Stern, R. J., Baes, M., Sobolev, S. V., & Whattam, S. A. (2015). Plate tectonics on the Earth triggered by plume-induced subduction initiation. *Nature*, 527(7577), 221–225. <https://doi.org/10.1038/nature15752>
- Gose, W. A. (1983). Late Cretaceous-Early Tertiary tectonic history of southern Central America. *Journal of Geophysical Research*, 88(B12), 10585–10592. <https://doi.org/10.1029/JB088iB12p10585>
- Grand, S. P., van der Hilst, R. D., & Widiyantoro, S. (1997). Global seismic tomography: A snapshot of convection in the Earth. *GSA Today*, 7(4), 1–7.
- Hall, C. E., Gurnis, M., Sdrolias, M., Lavier, L. L., & Müller, R. D. (2003). Catastrophic initiation of subduction following forced convergence across fracture zones. *Earth and Planetary Science Letters*, 212(1-2), 15–30. [https://doi.org/10.1016/S0012-821X\(03\)00242-5](https://doi.org/10.1016/S0012-821X(03)00242-5)
- Hauff, F., Hoernle, K., Schmincke, H. U., & Werner, R. (1997). A Mid Cretaceous origin for the Galapagos hotspot: Volcanological, petrological and geochemical evidence from Costa Rican oceanic crustal segments. *Geologische Rundschau*, 86(1), 141–155. <Go to ISI>://WOS:A1997XB30200011
- Hauff, F., Hoernle, K., van den Bogaard, P., Alvarado, G., & Garbe-Schönberg, D. (2000). Age and geochemistry of basaltic complexes in western Costa Rica: Contributions to the geotectonic evolution of Central America. *Geochemistry, Geophysics, Geosystems*, 1(5). <https://doi.org/10.1029/1999GC000020>
- Hoernle, K., Hauff, F., & van den Bogaard, P. (2004). 70 m.y. history (139–69 Ma) for the Caribbean large igneous province. *Geology*, 32(8), 697. <https://doi.org/10.1130/G20574.1>
- Isozaki, Y., Maruyama, S., & Furuoka, F. (1990). Accreted oceanic materials in Japan. *Tectonophysics*, 181(1-4), 179–205. <Go to ISI>://WOS:A1990ED69300014
- Johnson, C. L., Constable, C. G., Tauxe, L., Barendregt, R., Brown, L. L., Coe, R. S., et al. (2008). Recent investigations of the 0–5 Ma geomagnetic field recorded by lava flows. *Geochemistry, Geophysics, Geosystems*, 9, Q04032. <https://doi.org/10.1029/2007GC001696>
- Johnston, S. T. (2001). The Great Alaskan Terrane Wreck: Reconciliation of paleomagnetic and geological data in the northern Cordillera. *Earth and Planetary Science Letters*, 193(3-4), 259–272. <Go to ISI>://WOS:000172954200001
- Kerr, A. C., Marriner, G. F., Tarney, J., Nivia, A., Saunders, A. D., Thirlwall, M. F., & Sinton, C. W. (1997). Cretaceous basaltic terranes in western Colombia: Elemental, chronological and Sr-Nd isotopic constraints on petrogenesis. *Journal of Petrology*, 38(6), 677–702. <Go to ISI>://WOS:A1997XJ21800001
- Kirschvink, J. L. (1980). The least-squares line and plane and the analysis of palaeomagnetic data. *Geophysical Journal International*, 62(3), 699–718. <https://doi.org/10.1111/j.1365-246X.1980.tb02601.x>

- Konrad, K., Koppers, A. A., Steinberger, B., Finlayson, V. A., Konter, J. G., & Jackson, M. G. (2018). On the relative motions of long-lived Pacific mantle plumes. *Nature Communications*, 9(1), 854. <https://doi.org/10.1038/s41467-018-03277-x>
- Koymans, M. R., Langereis, C. G., Pastor-Galán, D., & van Hinsbergen, D. J. J. (2016). Paleomagnetism.org: An online multi-platform open source environment for paleomagnetic data analysis. *Computers & Geosciences*, 93, 127–137. <https://doi.org/10.1016/j.cageo.2016.05.007>
- Kuijpers, E. P. (1980). The geologic history of the Nicoya Ophiolite Complex, Costa-Rica, and its geotectonic significance. *Tectonophysics*, 68(3–4), 233–255. <Go to ISI>://WOS:A1980KL67200007
- Leng, W., & Gurnis, M. (2011). Dynamics of subduction initiation with different evolutionary pathways. *Geochemistry, Geophysics, Geosystems*, 12, Q12018. <https://doi.org/10.1029/2011GC003877>
- Li, S., Advokaat, E. L., van Hinsbergen, D. J., Koymans, M., Deng, C., & Zhu, R. (2017). Paleomagnetic constraints on the Mesozoic–Cenozoic paleolatitudinal and rotational history of Indochina and South China: Review and updated kinematic reconstruction. *Earth-Science Reviews*, 171, 58–77. <https://doi.org/10.1016/j.earscirev.2017.05.007>
- Liu, L., Spasojevic, S., & Gurnis, M. (2008). Reconstructing Farallon plate subduction beneath North America back to the Late Cretaceous. *Science*, 322(5903), 934–938. <https://doi.org/10.1126/science.1162921>
- Liu, L., & Stegman, D. R. (2011). Segmentation of the Farallon slab. *Earth and Planetary Science Letters*, 311(1–2), 1–10. <https://doi.org/10.1016/j.epsl.2011.09.027>
- Madrigal, P., Gazel, E., Denyer, P., Smith, I., Jicha, B., Flores, K. E., et al. (2015). A melt-focusing zone in the lithospheric mantle preserved in the Santa Elena Ophiolite, Costa Rica. *Lithos*, 230, 189–205. <https://doi.org/10.1016/j.lithos.2015.04.015>
- Madrigal, P., Gazel, E., Flores, K. E., Bizimis, M., & Jicha, B. (2016). Record of massive upwellings from the Pacific large low shear velocity province. *Nature Communications*, 7(1), 13309. <https://www.ncbi.nlm.nih.gov/pubmed/27824054>, <https://doi.org/10.1038/ncomms13309>
- Maffione, M., Thieulot, C., van Hinsbergen, D. J. J., Morris, A., Plümper, O., & Spakman, W. (2015). Dynamics of intraoceanic subduction initiation: 1. Oceanic detachment fault inversion and the formation of supra-subduction zone ophiolites. *Geochemistry, Geophysics, Geosystems*, 16, 1753–1770. <https://doi.org/10.1002/2015GC005746>
- Maffione, M., & van Hinsbergen, D. J. (2018). Reconstructing plate boundaries in the Jurassic neo-Tethys from the east and west Vardar ophiolites (Greece and Serbia). *Tectonics*, 37, 858–887. <https://doi.org/10.1002/2017TC004790>
- Matsuda, T., & Isozaki, Y. (1991). Well-documented travel history of Mesozoic Pelagic Chert in Japan—From remote ocean to subduction zone. *Tectonics*, 10(2), 475–499. <Go to ISI>://WOS:A1991FD98700014
- Molina Garza, R. S., van Hinsbergen, D. J., Boschman, L. M., Rogers, R. D., & Ganerød, M. (2017). Large-scale rotations of the Chortis Block (Honduras) at the southern termination of the Laramide flat slab. *Tectonophysics*. <https://doi.org/10.1016/j.tecto.2017.11.026>
- Montero, W., Lewis, J. C., & Araya, M. C. (2017). The Guanacaste volcanic arc sliwer of northwestern Costa Rica. *Scientific Reports*, 7(1), 1797. <https://doi.org/10.1038/s41598-017-01593-8>
- Mullender, T. A., Frederichs, T., Hilgenfeldt, C., de Groot, L. V., Fabian, K., & Dekkers, M. J. (2016). Automated paleomagnetic and rock magnetic data acquisition with an in-line horizontal “2G” system. *Geochemistry, Geophysics, Geosystems*, 17, 3546–3559. <https://doi.org/10.1002/2016GC006436>
- Müller, R. D., Seton, M., Zahirovic, S., Williams, S. E., Matthews, K. J., Wright, N. M., et al. (2016). Ocean basin evolution and global-scale plate reorganization events since Pangea breakup. *Annual Review of Earth and Planetary Sciences*, 44(1), 107–138. <https://doi.org/10.1146/annurev-earth-060115-012211>
- Nokleberg, W. J. (2000). *Phanerozoic tectonic evolution of the Circum-North Pacific*. Denver: U.S. Dept. of the Interior, U.S. Geological Survey.
- O'Neill, C., Müller, D., & Steinberger, B. (2005). On the uncertainties in hot spot reconstructions and the significance of moving hot spot reference frames. *Geochemistry, Geophysics, Geosystems*, 6, Q04003. <https://doi.org/10.1029/2004GC000784>
- Phipps Morgan, J., Ranero, C. R., & Vannucchi, P. (2008). Intra-arc extension in Central America: Links between plate motions, tectonics, volcanism, and geochemistry. *Earth and Planetary Science Letters*, 272(1–2), 365–371. <https://doi.org/10.1016/j.epsl.2008.05.004>
- Pindell, J. L. (1985). Alleghenian reconstruction and subsequent evolution of the Gulf of Mexico, Bahamas, and Proto-Caribbean. *Tectonics*, 4(1), 1–39. <Go to ISI>://WOS:A1985AEJ4500001
- Pindell, J. L., Cande, S. C., Pitman, W. C., Rowley, D. B., Dewey, J. F., Labrecque, J., & Haxby, W. (1988). A plate-kinematic framework for models of Caribbean evolution. *Tectonophysics*, 155(1–4), 121–138. <Go to ISI>://WOS:A1988R523100006
- Pindell, J. L., & Kennan, L. (2009). Tectonic evolution of the Gulf of Mexico, Caribbean and northern South America in the mantle reference frame: an update. *Geological Society, London, Special Publications*, 328(1), 1.1–1.55. <https://doi.org/10.1144/SP328.1>
- Pons, J. M., Vicens, E., & Schmidt-Effing, R. (2016). Campanian rudists (Hippuritida, Bivalvia) from Costa Rica (Central America). *Journal of Paleontology*, 90(2), 211–238. <https://doi.org/10.1017/jpa.2016.27>
- Révilleon, S., Hallot, E., Arndt, N., Chauvel, C., & Duncan, R. (2000). A complex history for the Caribbean Plateau: Petrology, geochemistry, and geochronology of the Beata Ridge, South Hispaniola. *The Journal of Geology*, 108(6), 641–661. <https://doi.org/10.1086/317953>
- Rogers, R. D., Mann, P., & Emmet, P. A. (2007). Tectonic terranes of the Chortis block based on integration of regional aeromagnetic and geologic data. In *Special Paper 428: Geologic and tectonic development of the Caribbean plate boundary in northern Central America, The Geological Society of America Special Paper 428* (pp. 65–88).
- Sanchez, J., Mann, P., & Emmet, P. A. (2016). Late Cretaceous–Cenozoic tectonic transition from collision to transtension, Honduran Borderlands and Nicaraguan Rise, NW Caribbean Plate boundary. *Geological Society, London, Special Publications*, 431(1), 273–297. <https://doi.org/10.1144/SP431.3>
- Saunders, A. D., Tarney, J., Kerr, A. C., & Kent, R. W. (1996). The formation and fate of large oceanic igneous provinces. *Lithos*, 37(2–3), 81–95. <Go to ISI>://WOS:A1996UQ56100002
- Schmidt-Effing, R. (1979). Alter und Genese des Nicoya-Komplexes, einer ozeanischen Paläokruste (Oberjura bis Eozän) im südlichen Zentralamerika. *Geologische Rundschau*, 68(2), 457–494. <https://doi.org/10.1007/BF01820803>
- Sigloch, K., & Mihalynuk, M. G. (2013). Intra-oceanic subduction shaped the assembly of Cordilleran North America. *Nature*, 496(7443), 50–56. <https://www.ncbi.nlm.nih.gov/pubmed/23552944>, <https://doi.org/10.1038/nature12019>
- Sinton, C. W., Duncan, R. A., & Denyer, P. (1997). Nicoya Peninsula, Costa Rica: A single suite of Caribbean oceanic plateau magmas. *Journal of Geophysical Research*, 102(B7), 15507–15520. <https://doi.org/10.1029/97JB00681>
- Sinton, C. W., Duncan, R. A., Storey, M., Lewis, J., & Estrada, J. J. (1998). An oceanic flood basalt province within the Caribbean plate. *Earth and Planetary Science Letters*, 155(3–4), 221–235. <Go to ISI>://WOS:000072851700006
- Sinton, C. W., Sigurdsson, H., & Duncan, R. A. (2000). Geochronology and petrology of the igneous basement at the Lower Nicaraguan Rise, Site 1001. In R. M. Leckie, H. Sigurdsson, G. D. Acton, & G. Draper (Eds.), *Proceedings of the Ocean Drilling Program*, 165 *Scientific Results* (Chap. 15, Vol. 165, pp. 233–236).

- Stern, R. J. (2004). Subduction initiation: spontaneous and induced. *Earth and Planetary Science Letters*, 226(3-4), 275–292. [https://doi.org/10.1016/S0012-821X\(04\)00498-4](https://doi.org/10.1016/S0012-821X(04)00498-4)
- Stern, R. J., & Gerya, T. (2017). Subduction initiation in nature and models: A review. *Tectonophysics*, 746, 173–198.
- Stern, R. J., Reagan, M., Ishizuka, O., Ohara, Y., & Whattam, S. (2012). To understand subduction initiation, study forearc crust: To understand forearc crust, study ophiolites. *Lithosphere*, 4(6), 469–483. <https://doi.org/10.1130/L183.1>
- Tarduno, J. A., & Alvarez, W. (1985). Paleolatitudes of Franciscan limestones. *Geology*, 13(10), 741–741. <Go to ISI>:/WOS:A1985ASV7700017
- Tarduno, J. A., McWilliams, M., Sliter, W. V., Cook, H. E., Blake, M. C. Jr., & Premoli-Silva, I. (1986). Southern hemisphere origin of the cretaceous laytonville limestone of california. *Science*, 231(4744), 1425–1428. <https://www.ncbi.nlm.nih.gov/pubmed/17748086>, <https://doi.org/10.1126/science.231.4744.1425>
- Tauxe, L. (2010). *Essentials of paleomagnetism*. Berkeley: University of California Press.
- Tauxe, L., & Watson, G. S. (1994). The fold test—An Eigen analysis approach. *Earth and Planetary Science Letters*, 122(3-4), 331–341. <Go to ISI>:/WOS:A1994NK27600006
- Torsvik, T. H., Burke, K., Steinberger, B., Webb, S. J., & Ashwal, L. D. (2010). Diamonds sampled by plumes from the core-mantle boundary. *Nature*, 466(7304), 352–355. <https://www.ncbi.nlm.nih.gov/pubmed/20631796>, <https://doi.org/10.1038/nature09216>
- Torsvik, T. H., Smethurst, M. A., Burke, K., & Steinberger, B. (2006). Large igneous provinces generated from the margins of the large low-velocity provinces in the deep mantle. *Geophysical Journal International*, 167(3), 1447–1460. <https://doi.org/10.1111/j.1365-246X.2006.03158.x>
- Torsvik, T. H., Van der Voo, R., Preeden, U., Mac Niocaill, C., Steinberger, B., Doubrovine, P. V., et al. (2012). Phanerozoic polar wander, palaeogeography and dynamics. *Earth-Science Reviews*, 114(3-4), 325–368. <https://doi.org/10.1016/j.earscirev.2012.06.007>
- Tournon, J., & Alvarado, G. (1997). Mapa geológico de Costa Rica: Escala 1: 500000. *Editorial Tecnológica de Costa Rica*.
- van der Meer, D. G., Spakman, W., van Hinsbergen, D. J. J., Amaral, M. L., & Torsvik, T. H. (2010). Towards absolute plate motions constrained by lower-mantle slab remnants. *Nature Geoscience*, 3(1), 36–40. <https://doi.org/10.1038/ngeo708>
- van der Meer, D. G., Torsvik, T. H., Spakman, W., van Hinsbergen, D. J. J., & Amaral, M. L. (2012). Intra-Panthalassa Ocean subduction zones revealed by fossil arcs and mantle structure. *Nature Geoscience*, 5(3), 215–219. <https://doi.org/10.1038/ngeo1401>
- van der Meer, D. G., van Hinsbergen, D. J., & Spakman, W. (2018). Atlas of the Underworld: Slab remnants in the mantle, their sinking history, and a new outlook on lower mantle viscosity. *Tectonophysics*, 723, 309–448.
- van Hinsbergen, D. J. J., Steinberger, B., Doubrovine, P. V., & Gassmüller, R. (2011). Acceleration and deceleration of India-Asia convergence since the Cretaceous: Roles of mantle plumes and continental collision. *Journal of Geophysical Research*, 116, B06101. <http://doi.org/10.1029/2010JB008051>
- van Velzen, A. J., & Zijdeveld, J. (1995). Effects of weathering on single-domain magnetite in Early Pliocene marine marls. *Geophysical Journal International*, 121(1), 267–278. <https://doi.org/10.1111/j.1365-246X.1995.tb03526.x>
- Venable, M. E. (1994). A geologic, tectonic and metallogenic evaluation of the Siuna terrane. PhD Thesis, The University of Arizona.
- Wessel, P., & Kroenke, L. W. (2008). Pacific absolute plate motion since 145 Ma: An assessment of the fixed hot spot hypothesis. *Journal of Geophysical Research*, 113, B06101. <https://doi.org/10.1029/2007JB005499>
- Wessel, P., & Kroenke, L. W. (2009). Observations of geometry and ages constrain relative motion of Hawaii and Louisville plumes. *Earth and Planetary Science Letters*, 284(3-4), 467–472. <https://doi.org/10.1016/j.epsl.2009.05.012>
- Whattam, S. A., Gazel, E., Yi, K., & Denyer, P. (2016). Origin of plagiogranites in oceanic complexes: A case study of the Nicoya and Santa Elena terranes, Costa Rica. *Lithos*, 262, 75–87. <https://doi.org/10.1016/j.lithos.2016.06.017>
- Whattam, S. A., & Stern, R. J. (2015). Late Cretaceous plume-induced subduction initiation along the southern margin of the Caribbean and NW South America: The first documented example with implications for the onset of plate tectonics. *Gondwana Research*, 27(1), 38–63. <https://doi.org/10.1016/j.gr.2014.07.011>
- Wright, N. M., Seton, M., Williams, S. E., & Müller, R. D. (2016). The Late Cretaceous to recent tectonic history of the Pacific Ocean basin. *Earth-Science Reviews*, 154, 138–173. <https://doi.org/10.1016/j.earscirev.2015.11.015>
- Zijdeveld, J. D. A. (1967). A.C. Demagnetization of rocks: Analysis of results. In D. W. Collinson, K. M. Crees, & S. K. Runcorn (Eds.), *Methods in Paleomagnetism* (pp. 254–286). Amsterdam: Elsevier.